ABSTRACT

Title of Thesis:	COMPARATIVE ANALYSIS OF MINIATURE INTERNAL COMBUSTION ENGINE AND ELECTRIC MOTOR FOR UAV PROPULSION
	Branden Mark Chiclana, Mater of Science, 2017
Thesis Directed By:	Associate Professor, Dr. Christopher P. Cadou, Department of Aerospace Engineering

This thesis compares the performance of an engine/fuel tank based propulsion system to a motor/battery based propulsion system of equal total mass. The results show that the endurance of the engine/fuel system at the same thrust output is approximately 5 times greater than that of the motor/battery system. This is a direct result of the fact that the specific energy of the fuel is 20 times that of the lithium-polymer batteries used to power the motor. A method is also developed to account for the additional benefits of fuel consumption (and hence weight reduction) over the course of the flight. Accounting for this effect can increase endurance exponentially. Taken together, the results also demonstrate the dramatic performance improvements that are possible simply by replacing motor/battery systems with engine/fuel systems on small unmanned air vehicles.

COMPARATIVE ANALYSIS OF MINIATURE INTERNAL COMBUSTION ENGINE AND ELECTRIC MOTOR FOR UAV PROPULSION

by

Branden Mark Chiclana

Thesis submitted to the Faculty of the Graduate School of the
University of Maryland, College Park, in partial fulfillment
of the requirements for the degree of
Master of Science
2017

Advisory Committee:
Assoc. Professor Christopher Cadou, Chair
Assoc. Professor Kenneth Yu
Assoc. Professor Inderjit Chopra

Dedication

This is for all my family and friends who have supported me throughout my life and academic career. In addition, for all those who rise from disadvantaged backgrounds and looking to achieve the most in the life.

Acknowledgements

I would like to acknowledge my advisor Dr. Christopher Cadou for his support in my graduate career. In addition, I would like to thank Dr. Peter Kofinas and Dean Darryll Pines for their support and advice that fostered my academic approach and personal character.

I would like to thank my committee Dr. Kenneth Yu and Dr. Inderjit Chopra for helping me through this process.

I would like to thank the Aerospace Department , Leopoldo Torres, Dr. Winkelmann, Howie, and Mike for all their support, recommendations, and assistance throughout this journey.

I would like to thank Wiam Attar, Andrew Ceruzzi, Lucas Pratt, Dannish Maqbool, Steven Cale, Stephen Vannoy, Colin Anderson, and Jean-Luis Suazo for all the good times, support, and love.

Last, but never the least, I want to thank and say that I am grateful for my mom, family and close friends for all the love and support though all the tough moments. I could have not done it without you.

Table of Contents

List of Tables

List of Figures

List of Illustrations

If needed.

List of Nomenclature

C_{P_o}	Coefficient of Power
C_{T_o}	Coefficient of Thrust
ESC	Electronic Speed Controller
V	Volts
S	Cells for a LiPo battery
A	Ampere
mV	Milli-volts
wc	Water Column
E	Energy
P	System Power
η_o	Overall Efficiency
t	Endurance
E^*	Battery Specific Energy
Q_R	Fuel Specific Energy
M	Mass
g	Gravity
R	Range
L/D	Lift/Drag
C	Correction Coefficient
Kg	Kilogram
T	Thrust
D	Diameter of Propeller
n	Speed of Propeller
ρ_{ATM}	Atmosphere Density
K_v	RPM per volt
P_{prop}	Propeller Power
ICE	Internal Combustion Engine
$HCCI$	Homogeneous Charge Compression Ignition

Chapter 1: Introduction

1.1.0: Motivation

1.1.1: Fuel Powered Engines to Electric Powered Motors

The first objective of this research is to demonstrate the performance loss incurred by using electric motor/battery systems to power small unmanned air vehicles (UAVs). Batteries and hydrocarbon fuels have powered UAVs for commercial and military applications since the early 1900's[1–3]. However, consumers favor battery operated UAVs or motors because the system is user-friendly and convenient compared to hydrocarbon UAVs or engines. To power the motor, the assigned battery is simply connected to the motor and further operated with a remote control. In contrast, operating the engine takes knowledge and skill. The user needs to know how internal combustion engines (ICE) works and applying the proper throttle and needle valve settings. In addition, these engines are notoriously known to be noisy and messy, which can be an issue in residential communities. Despite the challenges with miniature engines they do have huge benefit. Battery operated UAVs suffer in endurance and power compared to hydrocarbon fuels because of its specific energy. Current battery technology is not capable of storing the same amount of energy as hydrocarbon fuels without making the unit heavy. In addition, unlike the engine, the weight of the power plant never dissipates as the energy is depleted. Therefore, as the battery depletes in energy it needs to supply more power for the same load. Thus, decreasing the efficiency of the system. Continuing, because of the motors flaw, as UAVs increase in size their power source are hydrocarbon fueled engines.

Hydrocarbon fuels allow UAVs to achieve greater endurance and power for its application.

1.1.3: Optimizing Conditions with Propellers

The third objective is to understand how to choose optimum propellers for small engines. Commercial engine manufactures give instructions on what propellers to use to "break-in" the engine and recommended propellers. However, they usually do not recommend propellers based on what the user would like to do – like maximize endurance, maximize climb performance, etc. We hope to provide some guidance in this regard for the engines considered here.

1.2.0: Previous Work

1.2.1: Performance Characteristics of OS 46 AX II

Shyam Menon measured the performance of nine miniature engines[4–7]. One of these was the OS 46 FX, which is the predecessor of the OS 46 AX II used here. Menon generated a performance map, peak performance ratings, and summary for the OS 46 FX. The power and efficiency results are used to understand how the engine operates for various fuel settings. Figure 1.1, Figure 1.2, and Figure 1.3 show the figures that Menon generated in his dissertation.

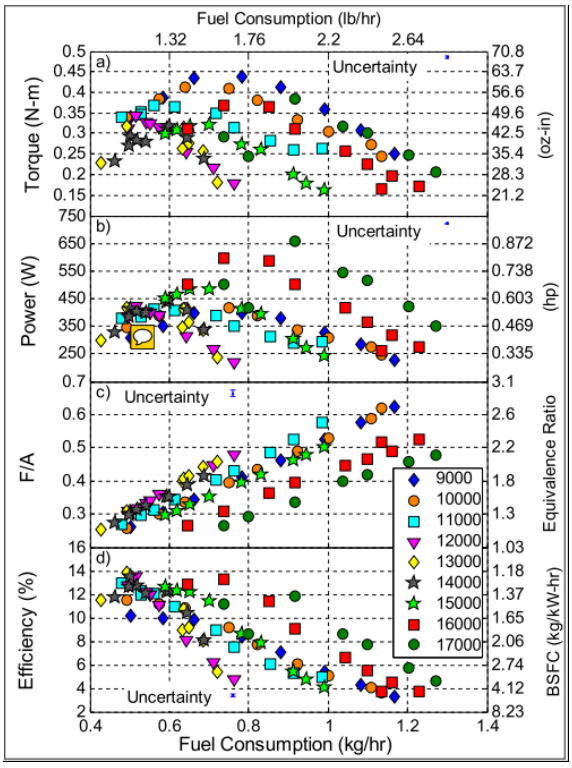

Figure 1.1: Menon's performance map of OS 46 FX

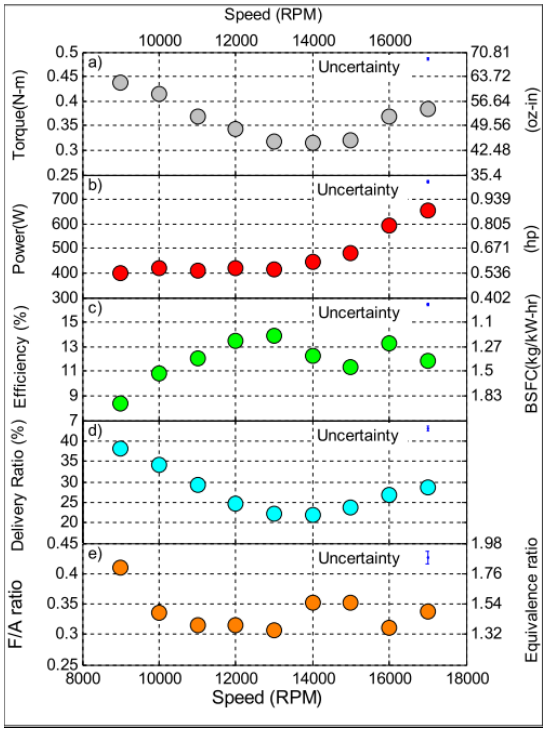

Figure 1.2: Menon's peak performance for OS 46 FX

Engine model			OS 46 FX		
Engine manufacturer			OS Engines		
Displacement	7.54 cc		0.46 cu.in.		
Bore	22 mm		0.87 in.		
Stroke	19.6 mm		0.77 in.		
Mass	488 g		17.21 oz.		
Geometric compression ratio	16.5				
	Value	**Units**	**@ rpm**	**@ F/A ratio**	**Uncertainty**
Peak torque	0.437	N–m	9000	0.41	4.7e–3
	61.88	oz–in	9000	0.41	0.66
Peak power output	681.09	W	17000	0.34	8.3
	0.913	hp	17000	0.34	0.011
Overall efficiency @ peak power	11.79	%	17000	0.34	0.15
BSFC @ peak power	1.39	kg/kW–hr	17000	0.34	0.02
Peak delivery ratio	38.42	%	9000	0.26	2.05
Peak normalized power	67.9	W	9000	0.41	0.75
Peak BMEP	353.13	kPa	9000	0.41	3.89
	51.22	psi	9000	0.41	0.56

Figure 1.3: Menon's summary of the O.S 46 FX

1.2.2: Performance Characteristics of Master Airscrew Propellers

Michael Selig is from the University of Illinois at Urbana-Champaign. Selig has made careful measurements[8,9] of the performance of a large number of commercial available small propellers and has made all of the data available on the UIUC Propeller Data Site[10]. Master Airscrew is one of the commercial propeller brands that is listed in the database. Coefficient of static thrust (C_{T_o}) and power (C_{P_o}) are used to predict thrust and output power from the engine and motor. Figure 1.4 and Figure 1.5 are examples of the coefficient plots.

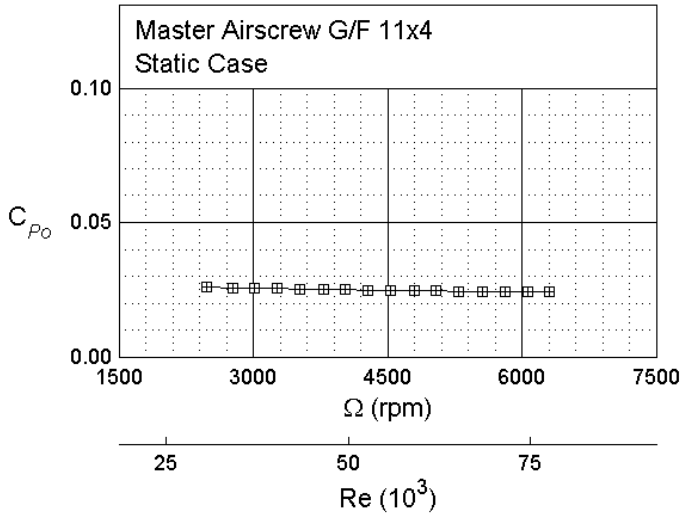

Figure 1.4: Master Airscrew 11x4 Cpo plot

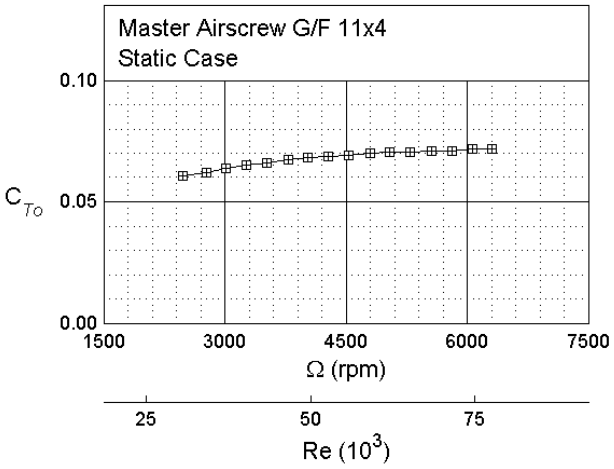

Figure 1.5: Master Airscrew 11x4 Cto plot

1.3.0: Objective and Approach

The objective of this work is to directly compare the endurance of engine/tank propulsion systems to battery/motor propulsion system under equal (ie. apples-to-apples) conditions. This is accomplished by attaching an engine and electric motor

on opposite ends of a bar. The bar pivots about an axis that is equidistant from and perpendicular to the thrust axes of the engine and motor as illustrated in Figure 1.4.

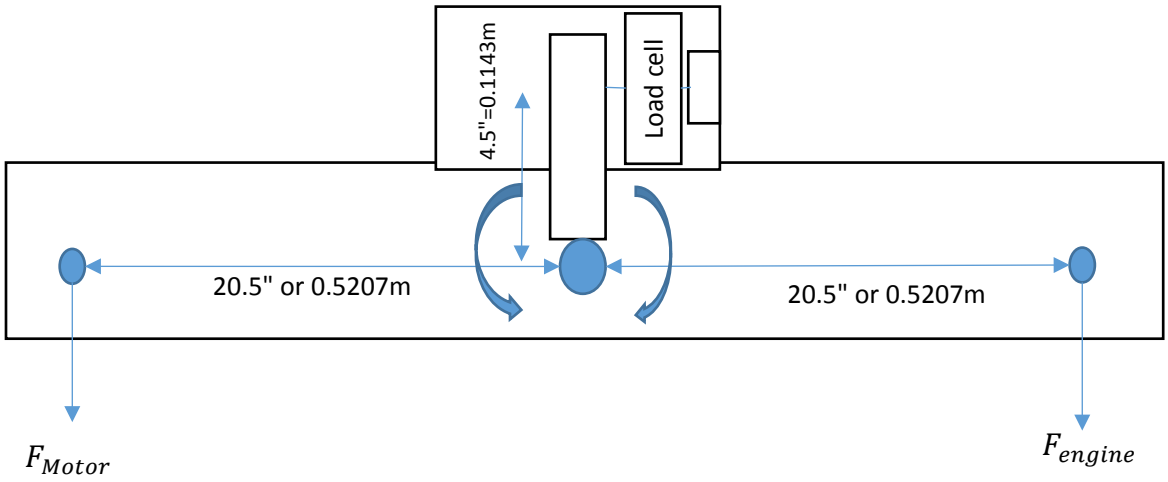

Figure 1.4: Diagram of the test stand

A load cell restrains the pivoting motion such that it reads zero when the engine and its propeller are producing the same thrust as the motor and its propeller. Fuel is added to the engine/tank system until it has the same mass as the motor/battery system. The engine and motor are started and run at the same thrust level (accomplished by adjusting the engine throttle such that the load cell output remains zero throughout the test) until one of the systems exhausts their power source. The time of battery and fuel exhaustion are measured. Other data like fuel flow rate, speed, ambient, cylinder head, and exhaust gas temperatures, and gas tank pressure are also measured in order to determine where the engine is operating in its operating map.

Chapter 2: System Operations

2.2.0 Engine Operations

2.2.1: HCCI Cycle Engines

Homogeneous Charge Compression Ignition (HCCI) are considered to be similar to diesel engines because they use high compression to initiate combustion and they can operate without a throttle[11,12]. HCCI uses a homogeneous fuel-air mixture that is created when fuel from the gas tank is mixed with air from the carburetor. This mixture is compressed in the chamber, which creates the combustion. Since HCCI is supposed to be a homogenous, the combustion process is uniform, which in return, does not create local rich areas[12].

HCCI engines can operate in two or four cycles. When operating in four cycle the piston will transition four times for one cycle as seen in Figure 2.1**Error! Reference source not found.**[13].

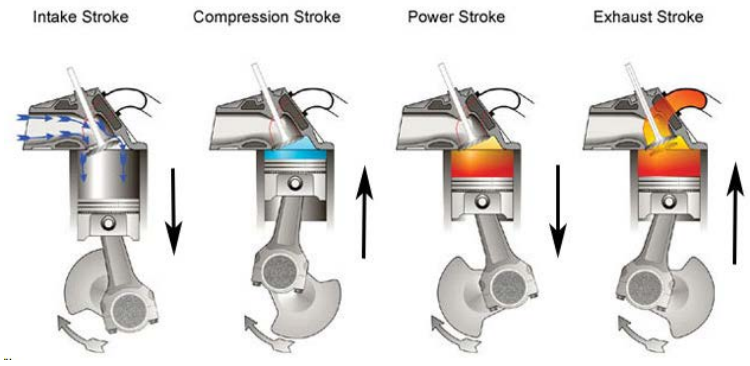

Figure 2.1: Engine Cycle Process

The intake phase, the piston transitions to bottom dead center (BDC) to let a fresh charge of air into the chamber. The compression phase, the piston translate toward

top dead center (TDC) compressing the air in preparation for combustion. Fuel will be sprayed in the chamber just before the piston reaches TDC to create a proper fuel-air mixture for combustion. The power phase, the piston is translating back to BDC and creating mechanical energy from the chemical reaction. The exhaust phase releases the exhaust from chamber in preparation for the next cycle.

When operating in two cycle the design allows it to combine the exhaust and power cycle as well as the intake and compression cycle. This improves the power to displacement ratio of the engine, but compromises the gas-exchange process due to the resultant breathing process [12]. The complication with this process is by reducing two cycles, the breathing process does not completely expel all the exhaust which is then mixed with the incoming fresh air charge. The mixture of exhaust and fresh air compromises the air-fuel ratio and combustion process.

2.2.2: Otto Cycle Engines

Otto cycle engines differ from HCCI or diesel engines because the combustion process is not completely dependent on compression. The compression ratio of an Otto cycle engine is too low to cause combustion solely. Therefore, when the piston is close to TDC a spark plug is used to initiate the combustion process.

2.2.3: Loop Scavenged Engines

Loop scavenged engines have similar characteristics like HCCI and Otto cycle engines. When the piston is TDC, glow fuel and air is pulled into the crankshaft as shown in Figure 2.2**Error! Reference source not found.**.

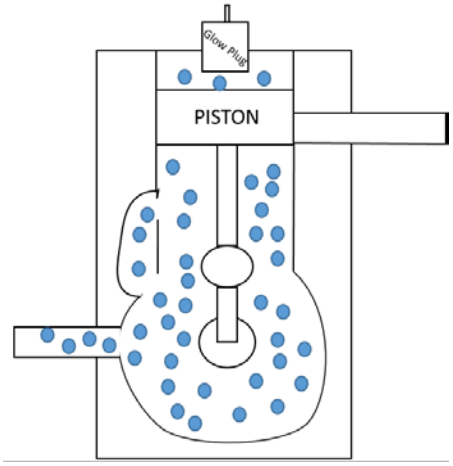

Figure 2.2: Diagram of a loop scavenged engine at TDC

The glow plug attached to the engine head has a platinum-coated spring inside that creates a chemical reaction with the methanol inside the mixture. This initiates combustion and the power stroke. As shown in **Error! Reference source not found.**, during the power stroke the piston covers the intake port thus creating a pressure differential or vacuum. When the piston reaches BDC, the port opens and does the following:

1) It introduces a fresh charge for the next cycle
2) The pressure differential assists in pushing the exhaust out of the chamber

Then the cycle restarts as shown in Error! Reference source not found.

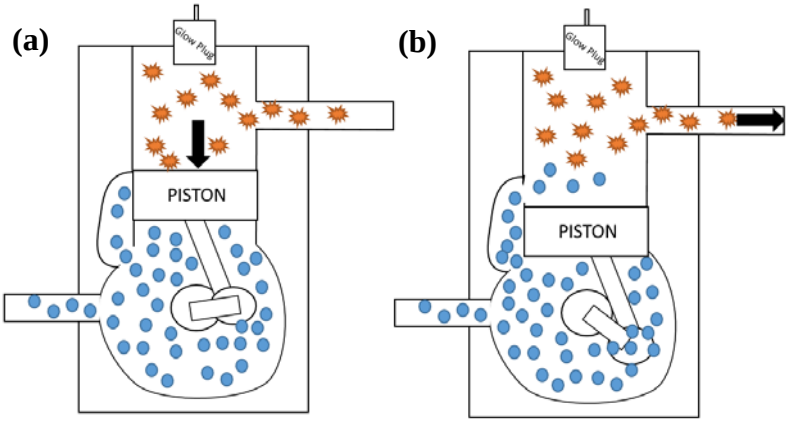

Figure 2.3: (a) Power Stroke and (b) Exhaust Cycle

The problem with this method is charge short-circuiting[11] . This occurs during scavenging when a fresh charge is introduced and it does not effectively push all the contaminates out for the next cycle. Thus, the following cycle will have some of the previous combustion exhaust in the current cycle. This will disrupt the engines performance because the cycle depends on the muffler to pressurize the gas tank that exerts a fuel flow rate to the engine. Therefore, this can reduce the efficiency significantly up to 35%[11].

2.2.4: Hydrocarbon Glow Fuel

The energy source for MAVs is called Glow Fuel. Glow fuel is a combination of nitromethane, methanol, and castor oil. Nitromethane is used because it contains oxygen to support the lack of atmosphere oxygen from the carburetor to have combustion. The methanol is used to create a catalytic reaction with platinum spring in the glow plug and start the combustion process. The castor oil is used for lubrication when the piston is translating during operation. A typical blend is 70% methanol, 20% oil and 10% nitromethane, which has an energy density of about 20 MJ/kg. While this is lower than other liquid hydrocarbons, it is still much greater than the best batteries[11]. The brand used is Cool Power by Morgan fuels that is shown in Figure 2.4.

Figure 2.4: Morgan Fuel's Cool Power Fuel

The composition of the fuel is 15% nitromethane, 17% lubrication, and 68% methanol. Since there was difficulty in getting this fuels specific energy it can be assumed that it is the same as Menon's value of 21.8 MJ/kg[11].

2.3.0 Motors

2.3.1: Motor Operation

Motors are similar to engines, in that, the purpose is to convert energy to produce work. However, the primary source of energy for motors is electricity. The electricity powers the magnets inside the motor to introduce magnetism. Magnetism is the opposing forces between north and south poles of magnets. When magnets of the same poles are held close they repel. However, if opposite poles are held close they will attract to each other. This concept is what allows the motor to generate rotation. There are two main parts to the design of motors: the rotor and the stator. The rotor

rotates to translate the work produced by the magnets and the stator is stationary. The orientation of the stator and rotor determines if the motor is brush or brushless. Figure 2.5[14] shows a diagram of a rotor and stator.

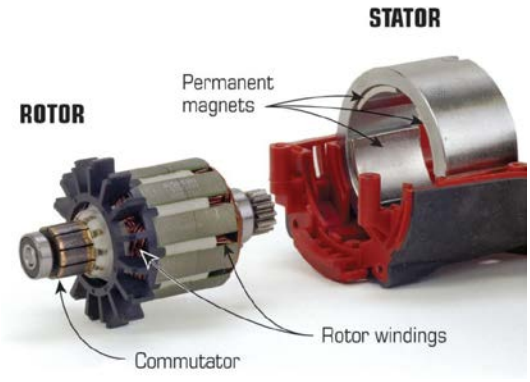

Figure 2.5: Motor rotor and stator

Depending on the design, the rotor or stator are constructed out of laminated steel shoes which allow copper wiring to go around them. The configuration on how the wire is wrapped around the shoes determines the strength or K_v of the motor.

A motor that has more winds with thinner wire around the shoes it will produce high RPMs. This type of motor will have a high K_v and would work best with smaller propellers. A motor that has less winds and thicker wire around the shoes would produce high torque. This type of motor will have a low K_v and work best with larger propellers. Motors are optimized by manipulating the timing of polarities. Referring to Figure 2.6, the rotor magnet is the same polarity as stator 1. However, stator 2 has the opposite polarity. This causes the stator 2 to pull and stator 1 to push. Once the magnet is over stator 2, stator 2 turns off and stator 3 is turned on with the opposite polarity as the incoming magnet. This technique delivers high efficiency because all the work being done contributes to one direction without any disruptions.

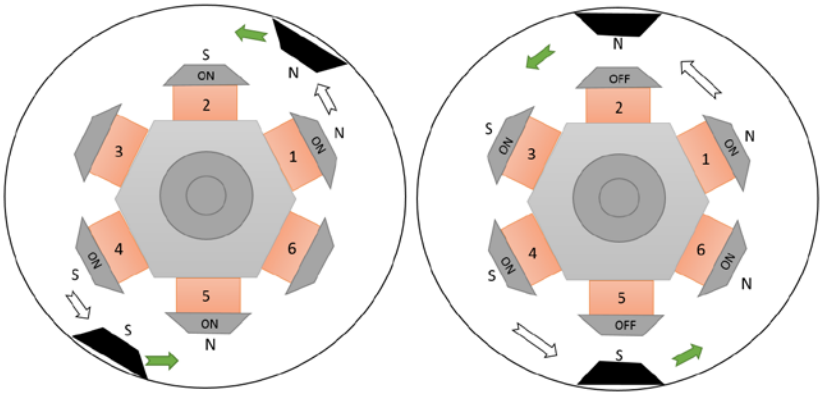

Figure 2.6: Operation of motor

2.3.2: Brush Motors

The first design for motors were brush style shown in Figure 2.5. For brush motors, the stator is on the outer part of the motor and the rotor is the inner. The name brush comes from the carbon “brushes” that connect with the commutator to apply power to the rotor shown in Figure 2.8.

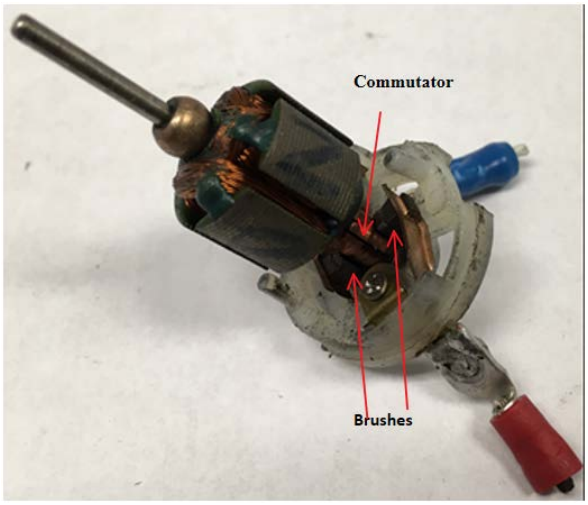

Figure 2.7: Brushes and armature for brush motor

Brush motors are great for applications for low reliability and lifespan. However, the design of brush motors are not efficient because a lot of power is lost due to the

friction from the brushes making contact with the commutator. A solution for this is to remove the brushes, which introduces brushless motors.

2.3.3: Brushless Motors

The thought behind brushless motors was to remove the friction that brushes generated. To do this, the design of brush motors is inverted so the stator is on the inner part of the motor and the rotor is the outer as shown in Figure 2.8[15].

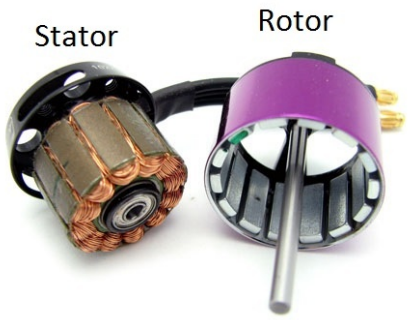

Figure 2.8: Brushless motor rotor and stator configuration

Now, the rotor is energized by magnetism instead of the brushes. This increases the efficiency and cleanliness of the motor while decreasing the temperature and risk. Brushless motors are used for high reliability and lifespan applications.

2.3.4: LiPo Batteries

Batteries are determined by what kind of material they are constructed from as well as the kind of electrolyte used to transfer electrons. A simple way to explain how batteries work is "[d]uring discharge, the negative electrode is the anode and the positive electrode is the cathode. Positive ions move from the anode to the cathode through the electrolyte and separator. Negative ions move in the opposite direction. The anode builds up negative charge and the cathode builds up positive charge,

creating the cell voltage V(t)"[16]. To charge the battery the process is reversed through oxidation and reduction reactions as shown in Figure 2.9[16].

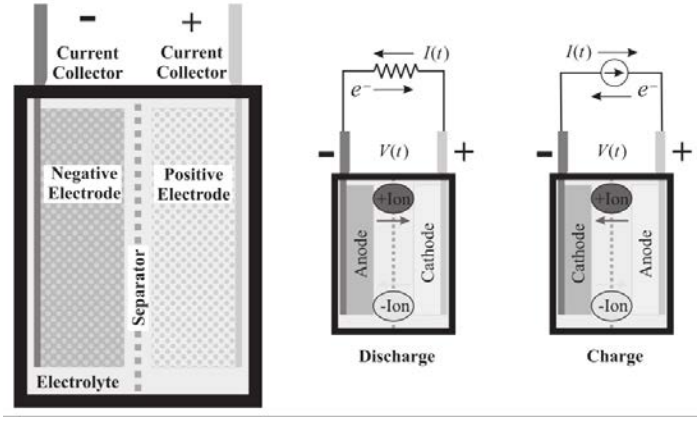

Figure 2.9: Discharge and charge of batteries

Lithium Polymer (LiPo) batteries are in the family of lithium-ion batteries. LiPo batteries can come in varies sizes ranging from 1*S* to 12S. These batteries are usually nominally charge, which is 3.7 V/S or can be peak charged to 4.2V/S. Also, they should never be discharged past 3.0 V/S because this can severely damage the battery. In addition, peak charging or discharging at a high rates are not recommended because they can shorten the lifetime of the battery. LiPo is preferred for UAV's or MAV's compared to other common batteries because they have a greater energy density. This factor is extremely important because having more energy in a smaller volume or lighter container does affect the efficiency and duration of flight. Table 2.1[16] emphasizes the benefits of using Li-ion compared to other common batteries for UAV applications.

	Pb–acid	Ni–MH	Li-ion
Theoretical			
Voltage (V)	1.93	1.35	4.1
Specific energy (Wh/kg)	166	240	410
Practical			
Specific energy (Wh/kg)	35	75	150
Energy density (Wh/L)	70	240	400
Coulometric efficiency	0.80	0.65–0.70	>0.85
Energy efficiency	0.65–0.70	0.55–0.65	~0.80
Specific power, 80% DOD (W/kg)	220	150	350
Power density (W/L)	450	>300	>800

Table 2.1: Battery Comparison

In addition, Figure 2.10[16] shows that LiPo batteries should be able to compete with ICE considering it shares a portion of ICE's performance region.

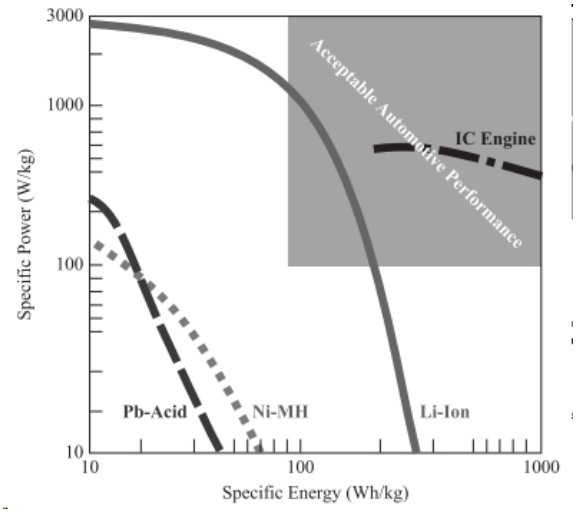

Figure 2.10: Specific power versus specific energy for batteries and ICE

Chapter 3: Apparatus and Experiments

3.1.0: Thrust Stand

Thrust stand reads the differential voltage output or thrust produced by both systems. The voltage output read by the load cell should always read ~0 volts (V) for the test to be accepted. The base needs to be heavy to oppose the moments from the systems. Figure 3.1 shows an aerial view of the thrust stand. On the west is the motor system, Turnigy G46 or G60, and on the east is the OS 46 AX. Behind the OS 46 AX is the exhaust hood that will collect the products, fumes and castor oil, that the engine releases. Figure 3.2 shows a close view of the load cell connection. The screw connected to the load cell is an eyebolt to ensure that the force translated to the load is linear when the bar is pivoted.

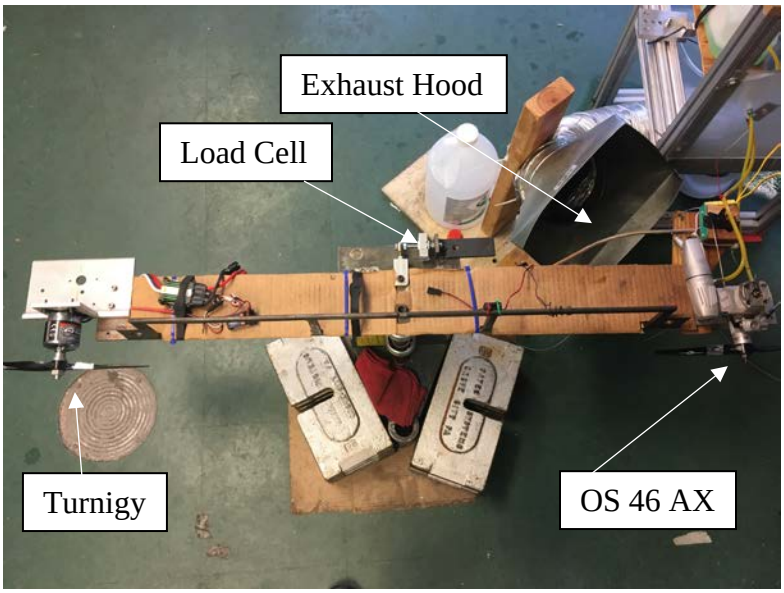

Figure 3.1: Aerial view of test stand set up

Figure 3.2: Close up view on load cell

3.2.0: Measurements

During the experiments, there are parameters that are being measured and recorded for both the OS 46 AX and Turnigy motors. For the engine, three thermocouples are used to collect ambient, exhaust, and engine head temperatures, two load cells are used to measure the weight of the fuel and thrust, one pressure transducer is used to measure the pressure of the fuel tank, and the tachometer is used to record the speed of the propeller. For the motor, an Electronic Speed Controller (ESC) is used to collect all the parameters such as speed, voltage, current, horsepower. Figure 3.3 and Figure 3.4 are block diagrams of the motor and engine system. The following sections will show how the parameters are measured.

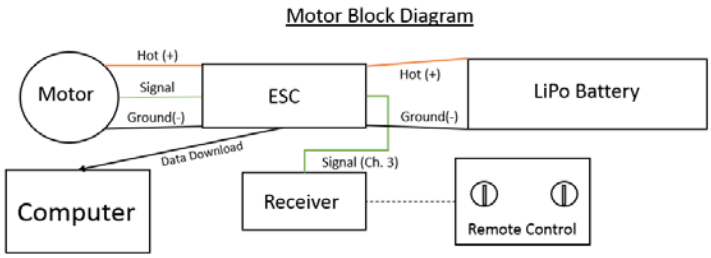

Figure 3.3: Motor block diagram

Figure 3.4: Engine block diagram

3.3.0: *Instrumentation and Measurements*

3.3.1: Data Acquisition System

To acquire all the data from the instrumentations a system is needed. National Instruments (N.I) have various devices that can acquire data from various sources.

The CompactDAQ (cDAQ) 9174 shown in Figure 3.5 is a chassis that enables and connects multiple modules to a computer. It is beneficial because it is capable of interfacing with various high performance module and is compact.

Figure 3.5: N.I. cDAQ-9174

The modules used with the cDAQ are NI 9205[17], NI 9213[18], and NI 9401[19]. The 9205 is a voltage module that can measure several voltage inputs in three voltage ranges. For the purpose of this research all the instrumentation connected to the 9174 are measured between $\pm$10 V. The NI 9213 is a thermocouple module that collects the three temperature readings. The NI 9213 is a counter module that reads a signal and converts it into a frequency. The frequency is manipulated to output the speed of the propeller.

3.3.2: Temperature Measurements

Three K-type thermocouples from Omega Engineering (KMQXL-040G-6) are used to measure the ambient, exhaust, and cylinder head temperature as shown in Figure 3.6. Then, the data read are sent to the 9213 and PC processing as shown Figure 3.4.

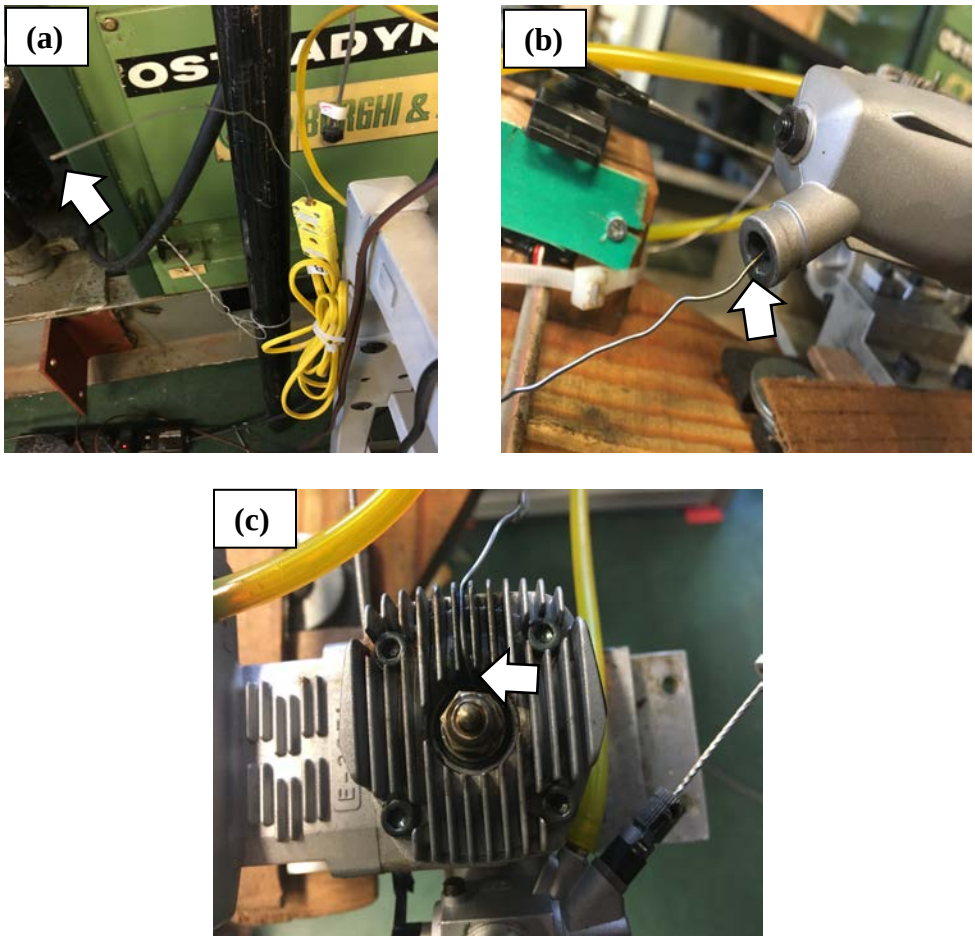

Figure 3.6: (a) Ambient, (b) exhaust, and (c) engine head thermocouples

3.3.3: Pressure Measurements

Shown in Figure 3.7, a hand-made water manometer connected to the gas tank for different RPMs was used to determine the range of muffler pressures to be expected. The tests showed that pressure transducer that can read 15"*wc* was needed. An Omega PX 277[20] was chosen to make this measurement. During testing the gas tank pressure will be monitored by the PX 277 and sent to the NI 9205 for further processing.

Figure 3.7: Hand-made water manometer to gas tank

3.3.4: Thrust Measurement

An OMEGA LCM703-25[21] load cell (full scale output at 15 lbf) is used to measure the thrust. The load cell outputs $\pm\, mV$ signals depending if the diaphragm inside is under compression or tension. If the engine is producing more thrust, the signal is negative (compression). However, if the motor is producing more thrust, the signal is positive (tension). Typically, the reading for the thrust load cell should always read ~0 mV because during the test both systems should output the same thrust. Having a load cell that can handle 25 pounds protects the diaphragm inside if one of the systems outputs a high load. A TMO-2 signal conditioner, shown in Figure 2.8, is used to amplify the signal to by a factor of approximately 100 so that it can be read by the data acquisition system.

3.3.5: Fuel Weight

The fuel weight is measured using a Trandsucer Techniques LSP-10[22] load cell with a full scale rage of 10 Kg. The LSP is a bending beam load cell that sends mV signals based on the deflection of its strain gauge. Another TMO-2 signal conditioner is used to amplify the output signal so it may be logged by the data acquisition system.

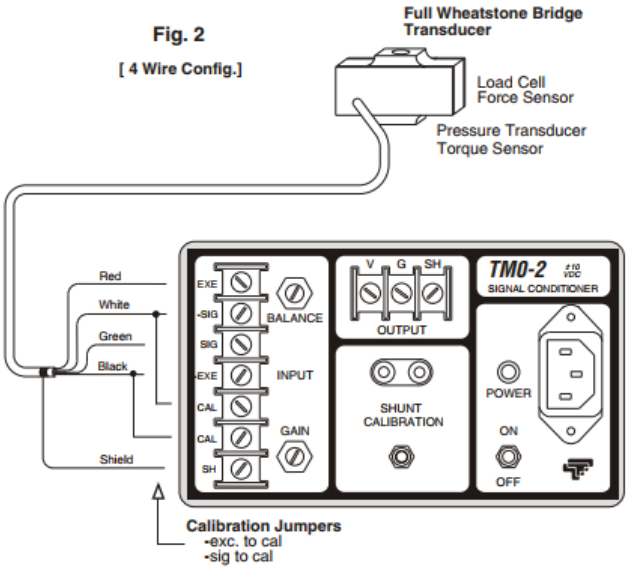

Figure 3.8: Transducer Techniques TMO-2 Signal Conditioner wire configuration

3.3.6: Speed

A ROS-W tachometer sensor from Monarch Instruments is used to record the frequency of the operating propeller shown in Figure 3.9

Figure 3.9: Monarch Instruments ROS-W tachometer

The sensor has an infrared light and detector that counts the time between two events and can operate between 1-250,000 rpm which covers the OS 46 AX II operating range (2,000-17,000 rpm). An event occurs each time the reflective tape on the propeller passes the infrared light produced by the tachometer. The count is sent to the 9213 as a square wave frequency, which can be transformed to RPM.

3.3.7: Motor Electronic Speed Controller

The Phoenix Edge 100 speed controller manufactured by Castle Creations, shown in Figure 10, is used in these experiments because it can power the two different motors and two different batteries (5S and 7S) that will be needed. The controller can handle input voltage range of 2-8V battery and up to 100*A* continuously. In addition, the Phoenix 100 is able to data log everything that occurs between the battery and the motor as mentioned in earlier.

Figure 3.10: Castle Creations Phoenix Edge 100

3.4.0: Calibration

The majority of all the instrumentation must be calibrated because of previous use or because of addition factors. The calibration process will be discussed for each instrumentation as follows: LCM703-25, LSP-10, PX 277, and the K-type thermocouples. The LCM703-25 and LSP-10 load cells are calibrated using known load calibration. Both load cells are connected to a TMO-2 using the 4-wire transducer configuration shown in Figure 3.8. In addition, a shunt connection is applied to avoid doing a known load calibration in the future. To create a shunt connection a resistor is plugged into the TMO-2 and –sig and +sig is connected to both “cal” screws. Using a 10V range, the LCM703-25 produces 0.88 V/Kg and the LSP-10 produces 1V/Kg. Once the load cells are connected to the TMO-2, a voltmeter is connected to the output and the known load calibration is performed as follows:

1) With no load applied, turn the balance until the load cell outputs ~ 0V

2) Apply a known load to the load cell. Turn the gain until the correct output voltage is displayed. Ex: for 1 Kg applied to the LCM703-25 the output should read 0.88V.
3) Unload and see if the voltage goes back to ~ 0V. If it does not output ~ 0 V, then repeat steps 1-3 until it does.
4) Once step is fulfilled, the shunt number will be acquired. With no load and known load, press the shunt button and record both numbers.
5) Confirm that NI 9205 reads the same as the voltmeter.

Since the measurements of the LSP-10 determines the fuel flow rate, the sensitivity of the calibration has to be capable of measuring a 1-gram change. Figure 3.11 shows LSP-10 being calibrated. In the first picture the gas tank and the carrier weigh 410g, as shown on the voltmeter. Then, 2g was applied and the voltage reads 412g.

(a)

(b)

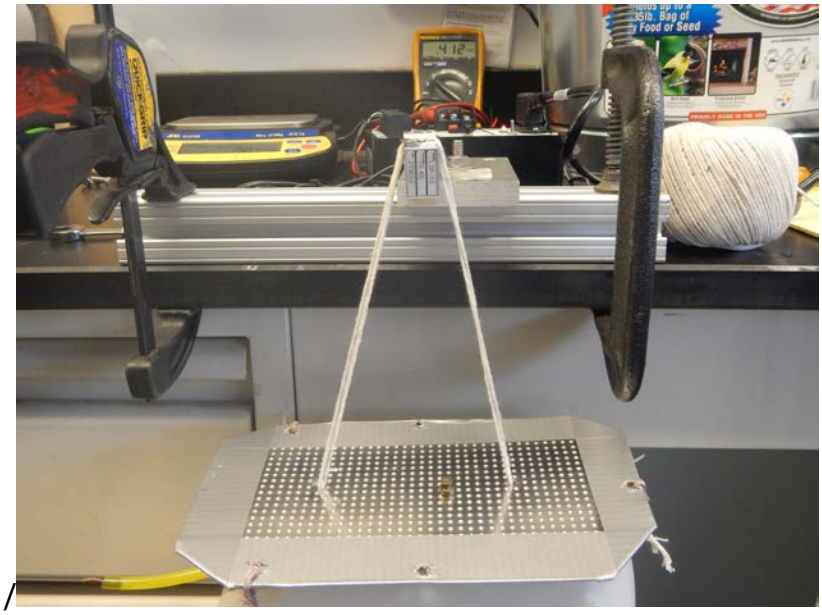

(C)

Figure 3.11: LSP-10 Calibration (a) Voltage reads 410g, (b) A 2g weight, (c) Voltage read 412g with 2g applied

The PX 277 pressure transducer is able to be calibrated in a similar fashion because it has its own version of a signal conditioner. A glass Y split, shown Figure 3.12, was purchased from the chemical department to connect the tank to the water manometer and PX 277.

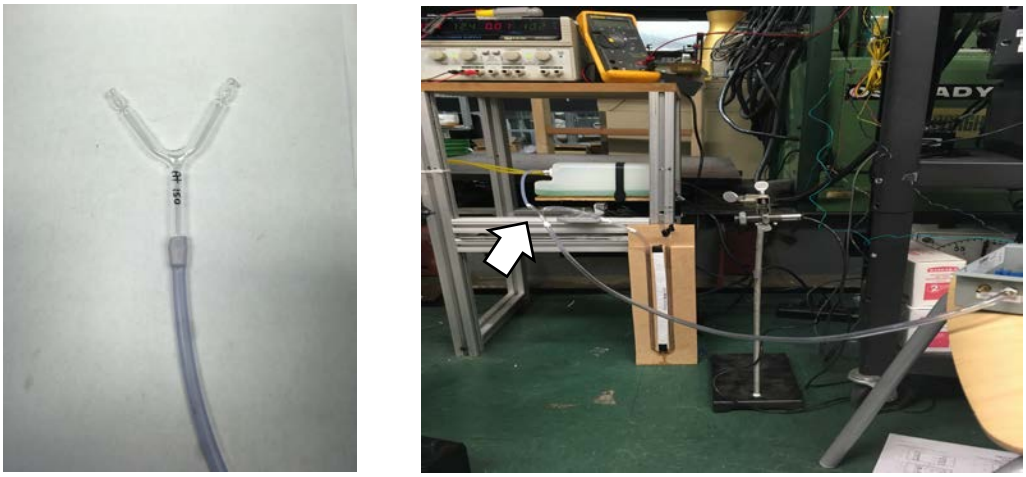

(A) **(B)**

Figure 3.12: (a) Glass Y split, (b) Photo of Y split connection

Also, Figure 3.13 shows a blueprint of the PX 277. A chart relating the relationship between *wc* and voltage output is created in excel. The configuration is set to 15" *wc*. A voltmeter is attached to the PX 277 and the following procedure as preformed to calibrate:

1) Turn the Zu to zero out to ~ 0 V
2) Once zero out, turn on engine. Let engine become stable on a RPM and read water manometer. Use the chart to see how much voltage the PX 277 should be outputting.
3) Turn the span or gain (S) to approximately the voltage on the chart. This is will be challenging because the engine is always fluctuating.

4) Change the speed of the engine and repeat step 3 one or two times to acquire data
5) Shut off engine and see if the engine comes back ~ 0 V. If not, then turn Zu to do so. If it does then leave it because it is zeroed properly.
6) Turn engine back on and try to achieve the same RPM before. Once achieved, see if the output is reading properly. If not, then perform step 3. If it does, then go to different RPM they you have not tried and see if the *wc* on manometer matches the voltage output on chart.
7) If 6 is accomplished, then they PX277 is calibrated. Once calibrated you can switch to any setting and it should convert.

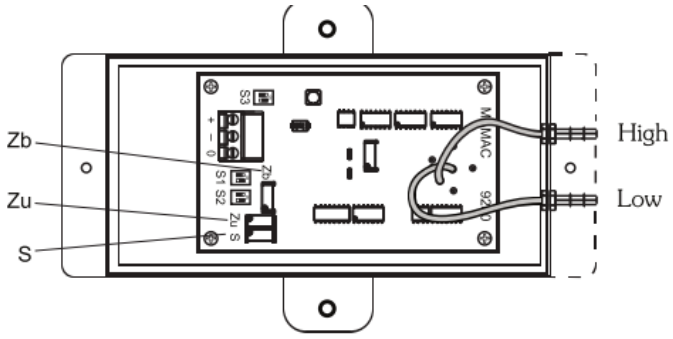

Figure 3.13: PX 277 component blueprint

The OMEGA K-type thermocouples are calibrated for the most part. It can also be challenging to create a calibration curve if various known temperatures cannot be applied. However, just to confirm that they are recording the correct values two known temperatures are applied. The first one was with ice. Ice is very close to 0℃ so if the thermocouples read this temperature it satisfies the lower operating range. The second one is boiling water. Boiling water is about 100℃. Once the water is boiling, the thermocouple is placed about an inch away from the bottom of the pot. It

is placed an inch away because the temperature of the water is desired not the pot temperature. If both test read close to 0℃ and 100℃ then the thermocouples are assumed to be calibrated and ready to be utilized.

3.5.0: Test Matrix

The foundation of this research will rely on endurance tests for constant propeller sizes and speeds for both systems. The propeller brand used is Master Airscrew and the style is the G/F model. The following propeller sizes are considered:

1) KN0906
2) KN1006
3) KN1008
4) KN1106
5) KN1104

The first two digits represent the propeller diameter in inches. The last two digits represent the pitch. The objective is to discover which system has the greatest endurance for the same operating conditions. The manufacture, OS Engine, advertises that the OS 46 AX II can operate from 2,000-17,000 rpm[23]. Engines are optimum when they operate in the upper RPM regime especially for these small engines. To obtain a broad performance map of this engine the target range will be from 6,000 to 17,000 rpm to cover a decent RPM spectrum.

Experiment	Engine				Motor		
	Model	Prop	Speed	Throttle	Model	Prop	Speed
1	OS46FX	11x4	10000	Var	1	11x4	10000
2	OS46FX	11x4	8000	Var	1	11x4	8000
3	OS46FX	9x6	13000	WOT	1	11x4	10000
4	OS46FX	11x4	12500	Var	2	11x4	12500
5	OS46FX	11x4	6000	Var	1	11x4	6000

Table 3.1: Propeller and Speed Test Matrix

3.6.0: Procedure

The process of collecting the data will be the following:

1) Choose the same propeller for both systems.
2) Choose a speed to operate both systems and confirm that both are producing the same thrust.
3) Perform the endurance test and collect all possible data.
4) The test will cease when one of the system stops or fails to provide the same amount of thrust as its opponent.
5) Repeat steps 2 and 4 to sweep through various speeds. Once the sweep is satisfied repeat step 1 with a different propeller.

The process of charging the Zippy Compact 5S and 6S batteries are the following:

1) Connect the LiPro Balance Charger (1) to a 12 V power supply.
2) Set the output voltage to 17.8 V and the output current to 3.33 A.
3) Connect the battery to the charger using the appropriate connectors.
4) Turn on the 12 V power supply to turn on the charger.

5) Set the mode to ‘LiPo Balance’ with an output of 2.5 A. If charging the 5S, set the voltage to 18.5 V. If the 6S, set to 22.2V.
6) Press enter and check if the charger is reading all the cells. If so press enter and charge the batteries. At this setting, the 5S should charge in ~30 mins and the 6S in ~50 mins.

For safety precautions, the following should be administered:

1) The batteries should be inserted in an explosion proof case (2). If there is an error with the battery and a chemical reaction does occur that leads to an explosion the bag should contain the effect.
2) Some of the chargers have timers that will stop the charging process. This will reduce the risk of overcharging the batteries
3) If the battery was just used for an operation, let the battery rest before charging to avoid further deterioration and possible explosion.

If the batteries are discharged, charged, and stored properly then the life cycle of the battery will maintain as designed from the company. However, if not treated in such manner the results can look like Figure 3.14. In Figure 3.14, the battery has blown up within the packaging. We can see this from the clear deformation of the battery. A key sign that a battery is going bad is when it begins to swell. Once this occurs, it is recommended to dispose the battery based on the regulations of your community.

Figure 3.14: Zippy Compact LiPo battery swollen

3.6.0: Uncertainty Analysis

There are two types of uncertainty: random error and systematic error[24]. Random error are fluctuations in measurements and occurs from the inability to reproduce the same measurements repeatedly. This error can be diminished by increasing the number of test or samples for the experiment because the error is a deviation around the mean. Systematic error is the error or inaccuracy that pertains to the instrumentation being used and its inability to perform repeated measurements. Finding the random error in the experiment the standard deviation about the mean, $S_{\bar{x}}$[24], is determined:

$$S_{\bar{x}} = \frac{S_x}{\sqrt{N}} = \sqrt{\frac{\sum_{i=1}^{N}(x_i - \bar{x})^2}{N-1}} * \frac{1}{\sqrt{N}}$$

where $\bar{x}$ is the mean of all the samples (N) and x_i is the measurement or sample for seach quantity of interest. The number of test performance for each case in this research is N=5. Finding the systematic error is determined by using the uncertainty,

linearity, and/or repeatability of the instrumentation and applying it to the following equation:

$$B_{\bar{x}} = \sqrt{\sum_{k=1}^{K} \left(b_{\bar{x}_k}\right)^2}$$

where K is the total number of systematic error and to $b_{\bar{x}_k}$ is an estimate of the standard deviation of K element[24].

Chapter 4: Engine-Propeller Matching

The overall objective in traditional engine-propeller matching (fixed pitch) is to find combinations of engines and propellers whose efficiencies peak at the same speed while producing the desired level of thrust at a desired vehicle speed. Since no vehicle is involved in this work, engine-propeller matching consists of finding the propeller whose torque-speed curve passes through the peak efficiency points in the engine (or motor) operating map.

4.1.0: Engine Operating Maps

An engine operating map is a plot of all possible combinations of torque and speed at which an engine can operate. A notional operating map is illustrated in Figure 4.1. The dotted and solid lines represent constant power curves for the engine. This is calculated by creating a matrix of torque times speed. The red and green line is generated from Menon's experimental peak efficiency and torque values from figure 1.2. The orange is the theoretical torque at peak which is calculated by multiplying speed with power. The baby blue, dark blue and purple lines are the torque curves for the 0906, 1006, and 1104 propellers. The 1006 and 1104 are shown as one curve

because they produce the same amount of torque. The purpose of generating this map is to hypothesize which propeller will work best with the engine and what the results will come out of it. Ideally, the propeller chosen should produce the greatest torque and efficiency. Analyzing the map it can be seen that the 0906 propeller intersects the second peak of the peak torque curve with an efficiency of ~10%. At lower speeds the 1006 and 1104 propellers can generate roughly the same results.

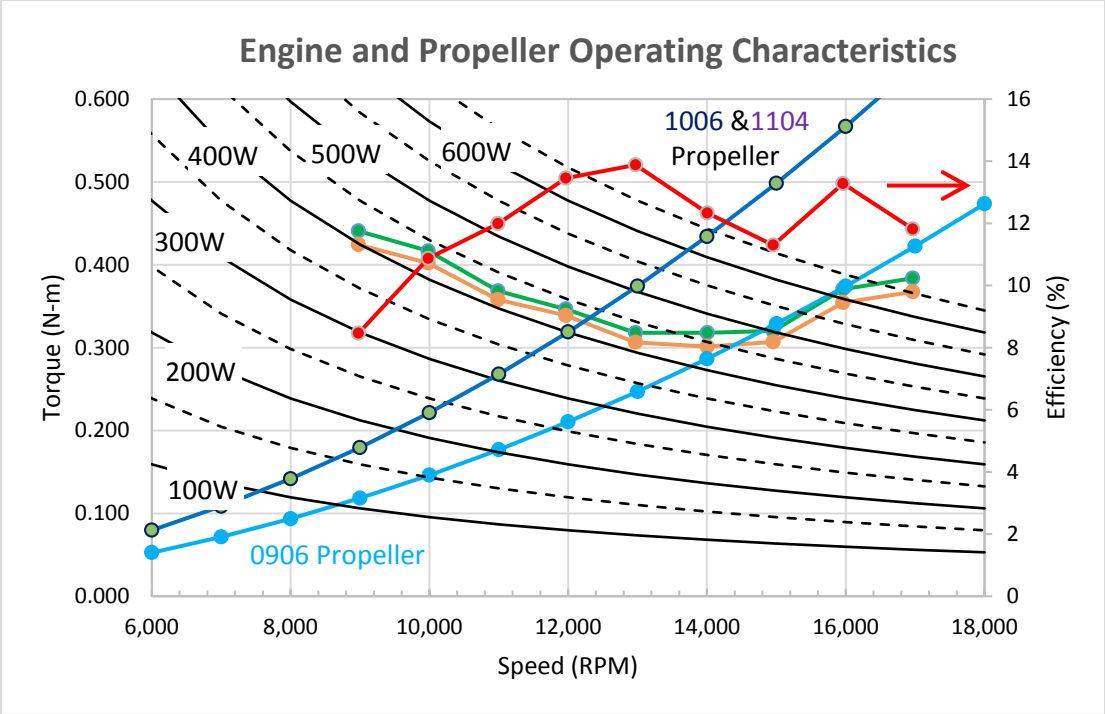

Figure 4.1: Engine and propeller operating map

4.2.0: Electric Motor Operating Maps

The Turnigy motors did not come with operating maps. To acquire the operating maps, both motors need to be tested on a dynamometer. However, the operating maps can still be briefly discussed in this section. There are two types of motor: Direct Current (DC) and Alternating Current (AC) induction. DC motors have a linear

relationship between torque and speed. When a constant load is applied, the speed is proportional to the applied voltage. Therefore, the results from a dynamometer should look like Figure 4.2[25] if the dynamometer is applying a known load and voltage is varied. Furthermore, in Figure 4.3, for the area inside of the torque curves there are a family of power curves. Referring to Figure 4.2, the recommended operating point for DC motor is located near the maximum power that can be achieved in Figure 4.3.

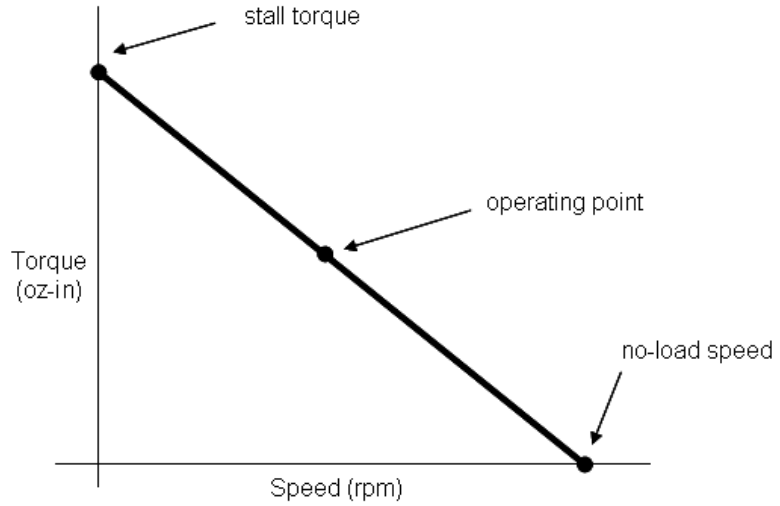

Figure 4.2: DC motor operating map

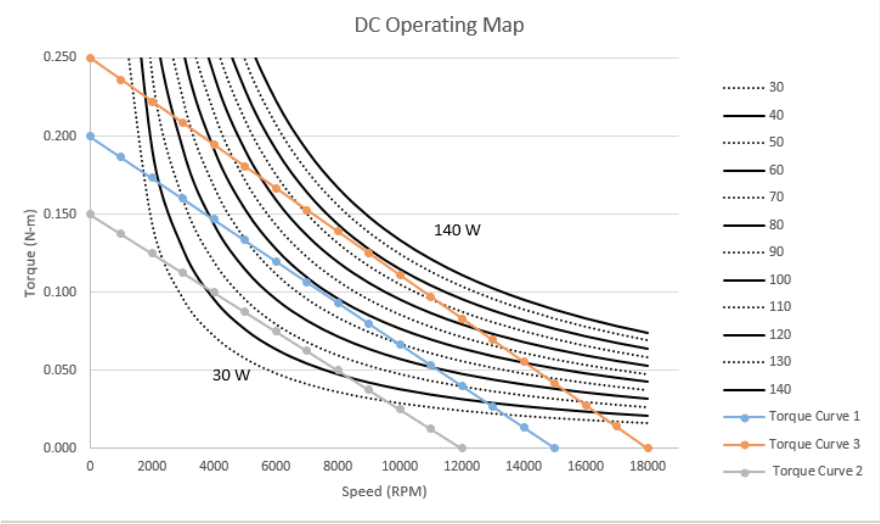

Figure 4.3: DC motor operating map with constant power curves

AC motors are different because of the three-phase shift. The Turnigy motors are AC induction motors. The relationship between torque and speed is not linear. Between 0% and 50% of maximum speed the torque with have a trough. Between 50% and 75% of the speed, the torque will increase to its peak value. Followed by a large torque decay as 100% of the speed is used. This behavior creates challenge to possess the same control as DC motors and finding the operating point. This is seen in Figure 4.3[26].

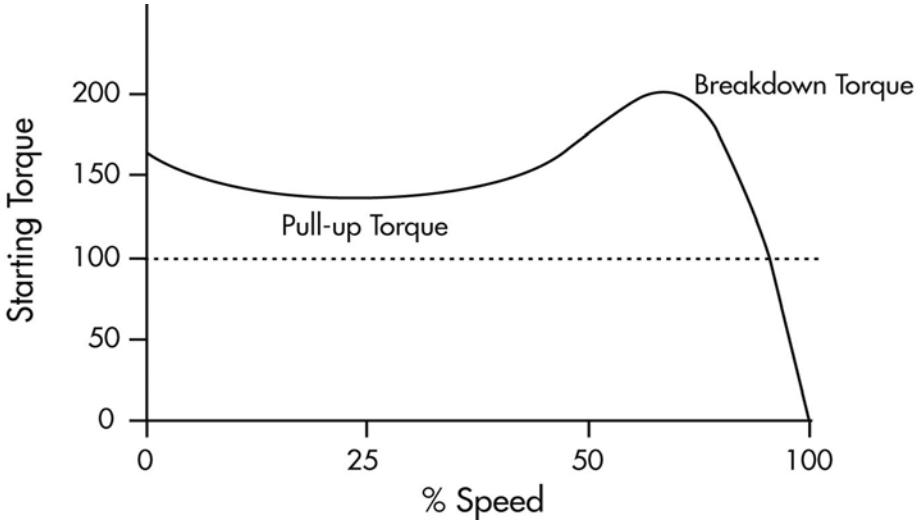

Figure 4.4: AC induction motor operating map

4.3.0: Propeller Operating Maps

To generate the propeller operating map Selig's database[10] must be used. The variables that is of interest is the static coefficient of power (C_{P_o}) and thrust(C_{T_o}) ,as shown in Figure 1.4 and 1.5, for each propeller of interest. We are acquiring the static data because both systems are static throughout test because they are attached to the thrust stand. Once the coefficients are obtained we can use the following equations to find the propellers power and thrust:

$$P_{prop} = C_{P_o}\rho_{atm}n^3D^5$$

$$T_{prop} = C_{T_o}\rho_{atm}n^2D^4$$

where ρ is the atmospheric density, n is the speed in rev/sec, and D is diameter of propeller in meters. Since the operating speed of the engine is from 2.5Krpm-17Krpm this array are applied to generate the power curves for each propeller. What the plot should show is as the diameter and pitch increase the propeller will produce more power and thrust. This could explain why the 1104 and 1006 have the same power and thrust because the diameter and pitch compensate and complement each other.

4.4.0: Overview of the Matching Process

A schematic illustration of the matching process is provided in Figure X. The operating point is the point where the power output of the engine equals that consumed by the propeller. While one can get a sense of where these points might be in FIGURE X, it is easier to see in Figure X1. Note that it may be possible for the engine's power output to match the propeller's demand at more than one speed. However, in order for this to be a physically realizable (ie. stable) operating point $\frac{dp_{engine}}{d\omega} < \frac{dp_{prop}}{d\omega}$ at the desired operating speed.

4.5.0: Selecting Propellers for the Test Matrix

We used measurements by Menon in the OS46FX to estimate the operating map of the OS46AX used here.

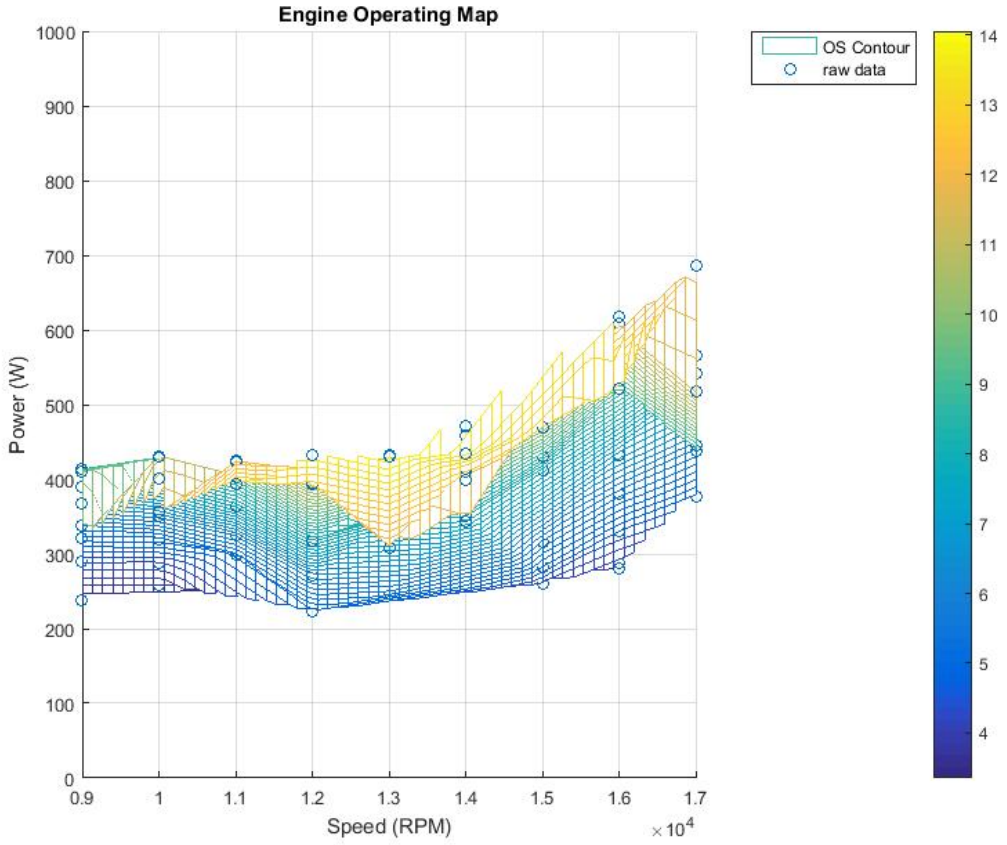

Figure 4.5: Engine Operating Map

Figure 4.4 is output power against speed of the OS46AX. The results shows a spectrum of where the engine would like to operate at different speeds. The blue circles are the raw due from Menon's data shown in figure 1.1. Then a mesh was applied to create the map. We can see that between 9Krpm and 14Krpm the engine can output between 250 W and 400 W of power. As the speed increases above 14Krpm, the power increases along with this. This can be due to the increase in

exhaust gas temperature and fuel flow rate to the engine. Also, looking at the color bar, the engine outputs more power when running efficiently. Therefore, the raw data points that are located in the yellow region are targeted for optimizing with the propeller. Figure 4.5 shows how the power consumption varies with speed for a variety of propellers. In order to choose the propeller that is best matched to the engine the OS 46 performance map is rendered in 3-D in Figure 4.6 so as to show power output and enabling one to visualize the propeller operating point

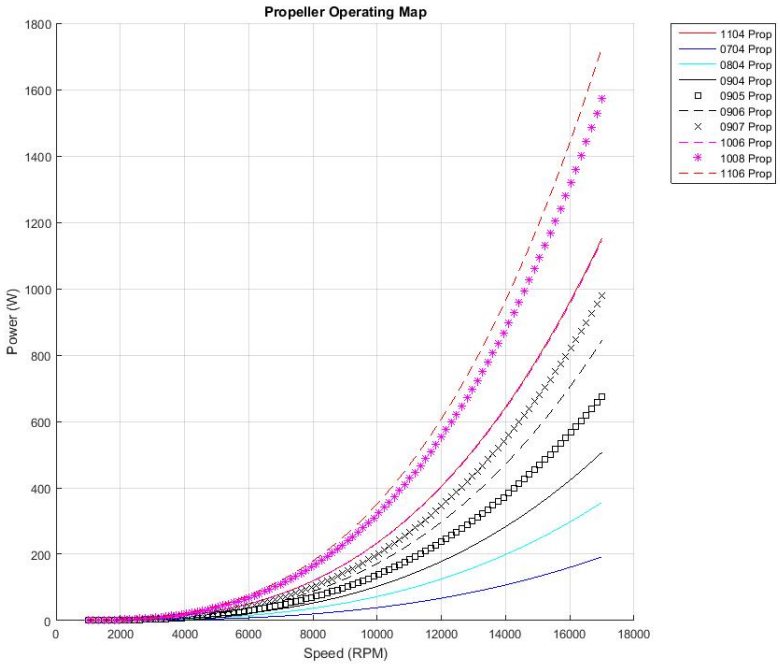

Figure 4.6: Operating map for various Master Airscrew propellers

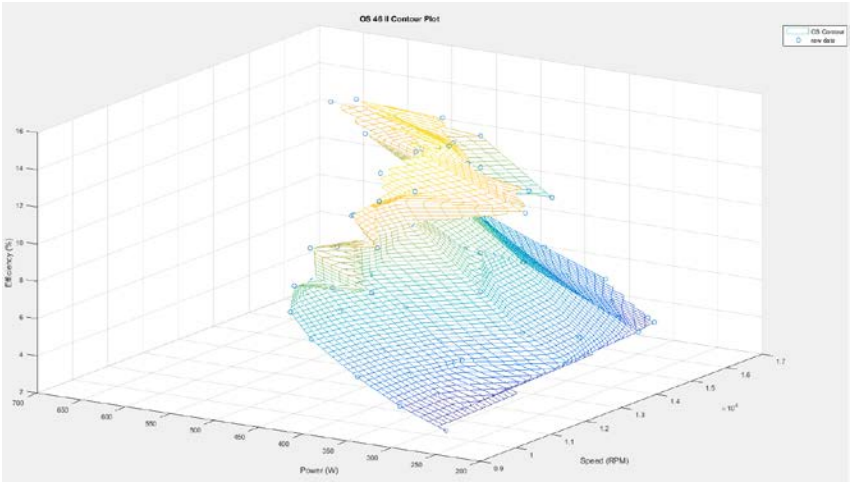

Figure 4.7: OS 46 Contour Performance Map

From Figure 4.7, the propellers that we are interested in are the KN1104, KN1006, and KN0905. The interest for the 1104 and 1006 is due two reasons:

1) Both the propellers have almost identical performance trends. Thus, it would be interesting to see which one is more efficient.
2) The propellers cross a point in the engine where the efficiency (denoted from the Z-axis) and the power are high.

The interest for the 0905 is due to it being the only propeller that sweeps through a large portion of the engines operating regime. Unfortunately, this propeller was not available so the 0906 will be used instead. This will be interesting because increasing the propeller pitch by one shows an approximate 200W increase at 17,000 RPM.

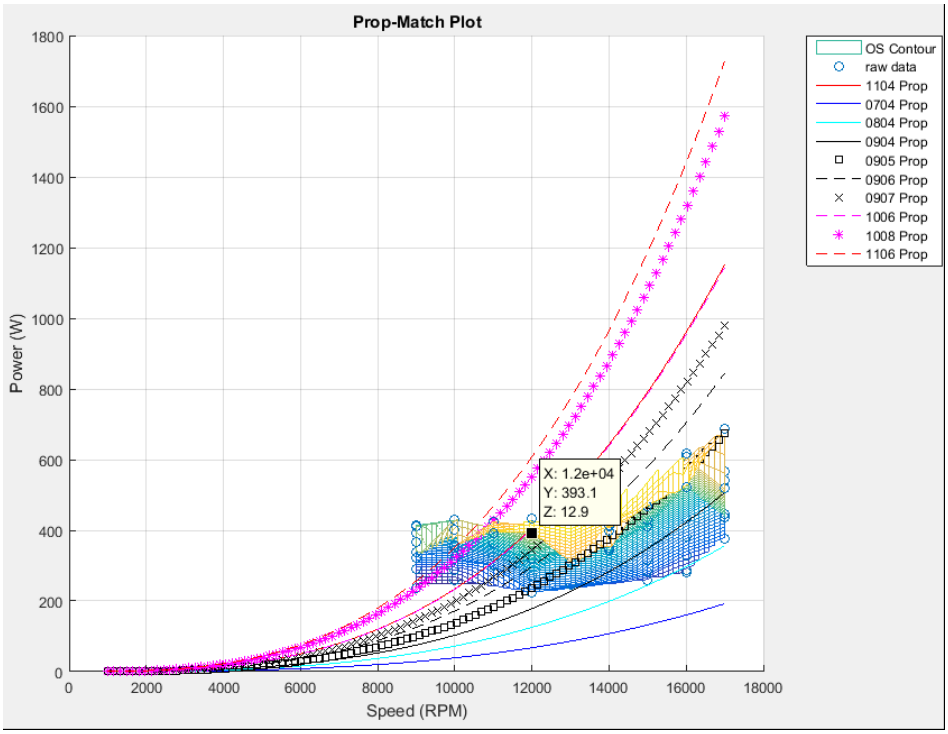

Figure 4.8: OS 46 Propeller Matching Performance Map

4.6.0: Data Analysis Procedure

It must be emphasized that (C_{P_o}) and (C_{T_o}) is estimated for this research because it is operating in higher RPMs then what Selig collected.

4.6.1: Data Acquisition Processing using LabVIEW

During each test, the engine instrumentation is collecting temperature, voltage, and frequency measurements from the thermocouples, load cells, and pressure transducer. All of the instrumentation are connected directly to its corresponding model, see figure __, except the load cells. The load cells signal output is in mV, which is too small and creates opportunity for error during processing .Therefore, the signal is amplified through signal conditioners to transform the signal from mV to V. Then, the output signal from the signal conditioner sent to the voltage module (NI 9205).

The measurements collected from all the instrumentation is sent through the cDAQ 9174 to be processed by LABview. The program written continuously acquires the data from the 9174 and processes the data through a series of product, the top box, and consumer, bottom box, loops as shown in Figure 4.8:

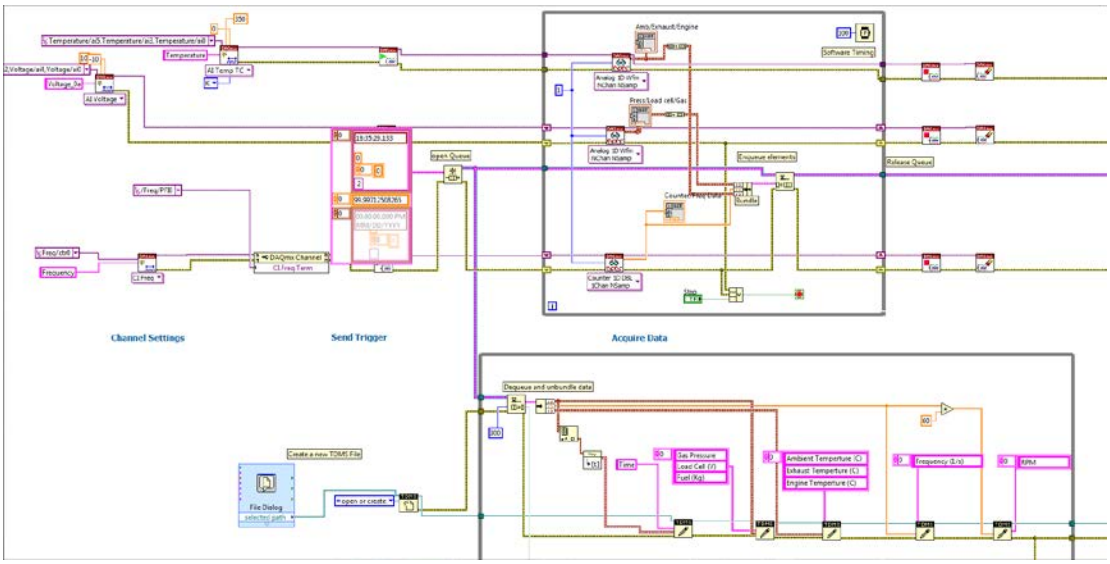

Figure 4.9: LabVIEW data processing program

When the test concludes, all the data is compiled into a TDMS file and saved in a designated folder for further processing. For the motor, collecting the measurements is fairly simple. The ESC is connected to the computer and, using the Castle Link program, downloads all the measurements to a separate excel spreadsheet.

4.6.2: Data Conversion and Organization Using Excel

The data in the TDMS can not be modified or edited. Thus, TDMS is converted to an excel spreadsheet to perform some small conversation and organization to be read in MATLAB. Knowing the duration of the experiment is of interest, but LabVIEW records the time in date and time format. This format will be transformed to a

standard time to interpret useful information. The conversion is done by taking the a specific point in time and subtracting the initial start time. This will give the duration in minutes and seconds. Another step is taken to transform the duration into second and milli-seconds to ensure precise timing of the test. The rest of the engine data will be processed using MATLAB. For the motor, the only conversion needed is the speed and time measurement. The speed measured is not the mechanical speed, but rather the electrical speed. The mechanical speed is the electrical speed divided by the number of magnetic poles in the motor. Both the G46 and G60 have a total of seven magnetic poles. Therefore, the electrical speed is divided by seven to obtain the mechanical speed of the motor. Even though the ESC is assigned to collect measurements at one sample per second time is not directly written to the spreadsheet. The next step is to make a new column for time and for each data point collected add a second. The rest of the motor measurements will be read using MATLAB. It is critical to compile all the excel spreadsheets for each case into a single spreadsheet to optimized the MATLAB code. For example, if a case using the 1004 propeller is performed, all the test performed with this propeller will be compiled into one spreadsheet using multiple tabs for each test.

4.6.3: Data Processing Using MATLAB

MATLAB is used to analyze all the compiled data for all the propeller cases. A code is written to access and read all the measurements for each propeller case and the various test within that case. The measurements collected are and used are in Table 4.1.

OS 46 AX II Data	Turnigy Motors
Time	Time
Gas Tank Pressure	Voltage
Thrust and Fuel Load Cell	Current
Temperature	Throttle Output
Speed	Speed
Engine System Weight	Motor System Weight

Table 4.1: Measurements collected and used

Another code was written to filter out any data that might contain any errors or does not meet designated constraints. For example, one of the constraints is the speed must be within five percent of the target speed. If a 1004 propeller case is performed with a target speed of 10 Krpm, any data that is not within 9.5 to 10.5 Krpm is not accepted for further analysis. From this filter, other filters will shape what data will be used for further analysis. The units are kept in SI units unless changed for simplicity. The pressure transducer is configured to handle 15" wc, which is 3732.6 Pa. The full scale voltage is 10V. Therefore, for each output volt there is 373.26 Pa in the gas tank. The fuel load cell is 10Kg load cell with 10V full range; 1 V/Kg. The calibration was set for 1g to equal 0.001 volts. Power of the battery, fuel, and propeller was calculated using the following formulas :

$$P_{battery} = I * V$$

$$P_{fuel} = SE_{fuel} * FFR$$

$$P_{propeller} = C_{p_o} * \rho * speed * D^5$$

where I is the current, V is the voltage, SE_{Feul} is specific energy of fuel, FFR is fuel flow rate, C_{p_o} is coefficient of power, ρ is density, speed is in rev/sec, and D is diameter of propeller in meters. The thrust parameters are found by the following

$$T_{selig} = C_{T_o} * \rho * speed * D^4$$

$$T_{Chiclana} = \frac{0.1143 * \frac{V}{0.88}}{0.5207} * 9.8$$

where V is the thrust load cell voltage. The specific energy of the battery is found by the following equation:

$$SE_{battery} = V * Ah$$

where V is the voltage and Ah is amp-hours. The units are wh/kg, which need to be converted to watts. This is achieved by multiplying the result by 3600. Finding the specific density of each system is the following:

$$SD_{battery} = \frac{SE_{battery}}{Vol}$$

$$SD_{Fuel} = \frac{SE_{Fuel} * Fuel\ Used}{Vol}$$

where vol is the volume of the battery or gas tank. The efficiencies are found by the following:

$$\eta = \frac{P_{output}}{P_{input}} * 100$$

$$BSFC = \frac{FFR}{P_{out}}$$

Chapter 5: Challenges

5.1.0: Instrumentation

The majority of the time for this research was spend troubleshooting because of unreliable instrumentation, repurposing resources, and making sure that all the instrumentation communicated properly. At first the NI SCXI was used to collect the measurements, however, using the SCXI become very complicated because of its outdated technology. The complication trickled down to writing a dense and complicated LABView code to filter and process the data.

Previously to the PX 277 pressure transducer, the PX 139 was used. It was difficult to used this product due to it's connection attachment. It consistently produced errors in the measurements. Also, a handmade 5V box was made to power the pressure transducer and other instruments. Due to abuse over the years, the box would smoke occasionally, which lead to re-wiring the entire box configuration.

A lot of the instrumentation used in this research did not have support or lack of information.

5.2.0: Engine Design Inconsistency

It was challenging to operate the engine for repeatable conditions. The engine's system is coupled to the pressure in the tank and exhaust temperature. If one parameter is influenced, the effects will disturb the engines speed and output power. In addition, the thread of the needle valve is fine. Therefore, it becomes difficult to make the needle valve setting repeatable without automation. Likewise, the throttle curvature makes repeatability challenging.

5.3.0: Engine Operating Inconsistency

Stable and unstable points occur when propeller matching for an engine. Sweeping through speeds for various propellers became challenging because the engine wants to operate at the stable points. Depending on the propeller attached, when attempting to operate for low speeds, the engine would want to accelerate to a higher speed regime. The most interesting speed is 8 Krpm because for any propeller the engine would transition back and forth from 8 Krpm to 9.5 Krpm. Therefore, 8 Krpm became a speed of interest for all propellers.

Chapter 6: Results

6.1.0: Individual Experiments

6.1.1: Thrust Measurements

Thrust was measured for the 0906, 1006, and 1104 propellers. When the test begins, the motor is not operating, thus giving the amount of thrust that the engine is producing. The motor is turned on to balance the load cell to ~0 V. With the load cell measuring ~0V, it can be said that the amount of thrust being produced by the motor is the same as the engine. Measured thrust is compared to Selig's thrust equation. This will be a good way to check the measured data acquired. Figure 6.1 shows the measured thrust produced for each test are located on the dotted black line, which represents the linear regression between the measured data and Selig thrust equation. Therefore, validates the measured thrust and the calibration of the load cell. The result also show the linear relationship between the propellers geometric construction

and speed. As the diameter or pitch is increased, the amount of thrust produced is increased. Comparing propeller 1006 and 1104, they produce the same thrust for various speeds because the diameter and pitch compensate to produce the same results. This is seen in Figure 4.7. There are some data points that are not exactly on the line, which can be a result of the small error in the load cell or friction from the thrust stand.

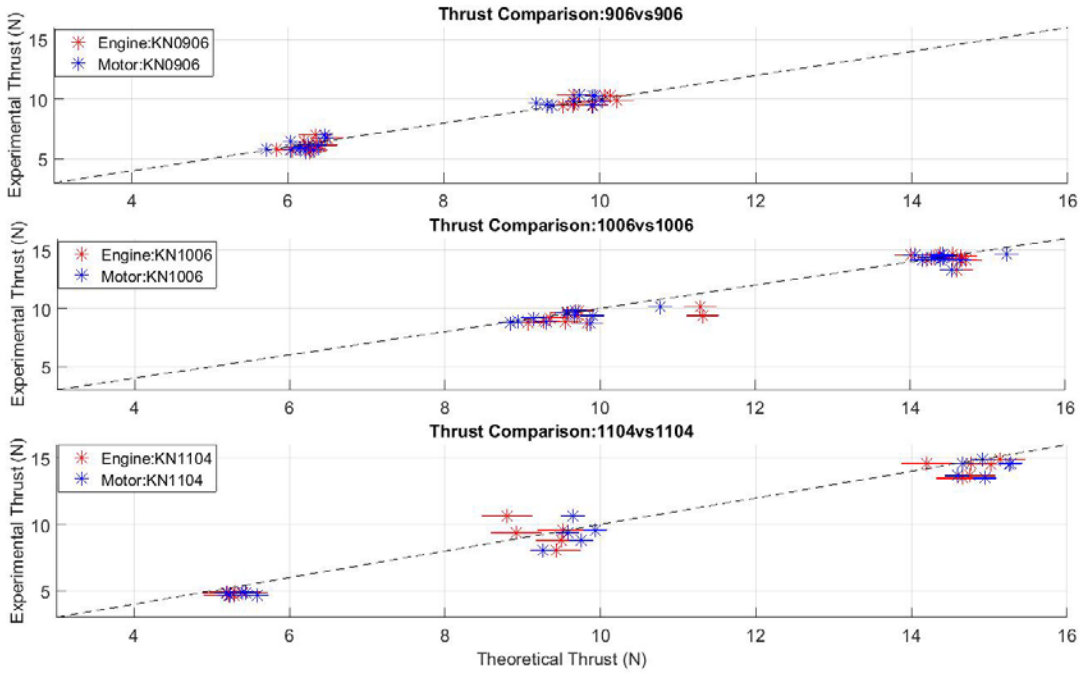

Figure 6.1: Thrust comparison for 0906, 1006, and 1004 propellers

6.1.2: Temperature Measurements

Figure 6.2 shows the ambient (blue), exhaust (red), and engine head (black) temperatures for the 0906, 1006, and 1104 propellers. The objective when running the engine was to attempt to have the highest exhaust temperature with the lowest engine head temperature. This is to ensure that the engine is running efficiently as possible while not running the risk of damaging the piston. Throughout all the test the

ambient temperatures remained about 300 °K. In the case of 8Krpm and below, it was challenging to have the exhaust temperature greater than the engine head temperature because at half throttle a large fuel flow rate is needed to slow the engine down to operate at that speed. In the case of 10Krpm, the exhaust and engine head temperatures are consistently between $350°K\ and\ 400°K$. The cause of this is due to a decrease in fuel flow rate, which allows the engine to combust the fuel more efficiently due to the engine approaching stoichiometric. Points greater than 10Krpm are the cases where the engine is optimized (slightly greater than stoichiometric) by achieving the greatest exhaust temperature and lowest engine head temperatures. The exhaust temperature increases above $450°K$ while maintaining the engine head temperatures similar to 10Krpm, which is result of increased efficiency. Greater endurance is the result of low fuel flow rate and high efficiency.

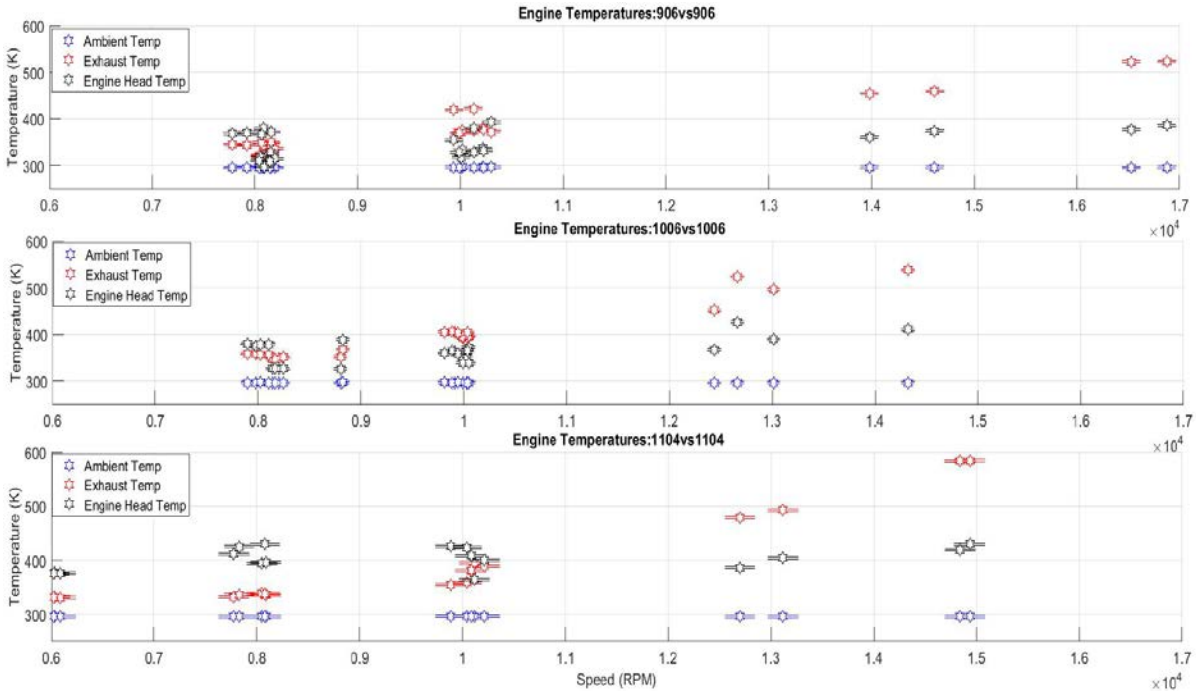

Figure 6.2: Temperature measurements at different speeds for 0906, 1006, 1104

6.1.3: Energy Density Measurements

The specific energy of hydrocarbon fuels are in the units J/Kg. However, batteries use the units Wh/kg, which Wh is a measure of voltage multiplied by amp hours. Amp hours (Ah) is a measure of discharge the battery can handle for an hour. Both batteries, 5S and 6s, have 5Ah. Compare both systems, Watt-hours is converted to J/Kg by multiplying by 3600. Figure 6.3 shows the comparison between the engine and motor energy density. The spread for the energy density data is the result of the amount of fuel used per test. Figure 6.3 a and b have similar results in that G46 5S battery has an energy of 6.5 and G60 6S battery has 8.3. Also, as the speed is increased the energy density is slightly decreased. This is can be due to the voltage demand at higher speeds. Figure 6.3c shows similar data as (a) and (b), but shows the result of peak charged batteries. When peak charging the 5S and 6S batteries, there is a 6% and 9% increase in their energy density. Considering the long-term damage due to peak charging this is a big trade off. Also, even when the batteries are peak charged they cannot compete with hydrocarbon fuels energy density.

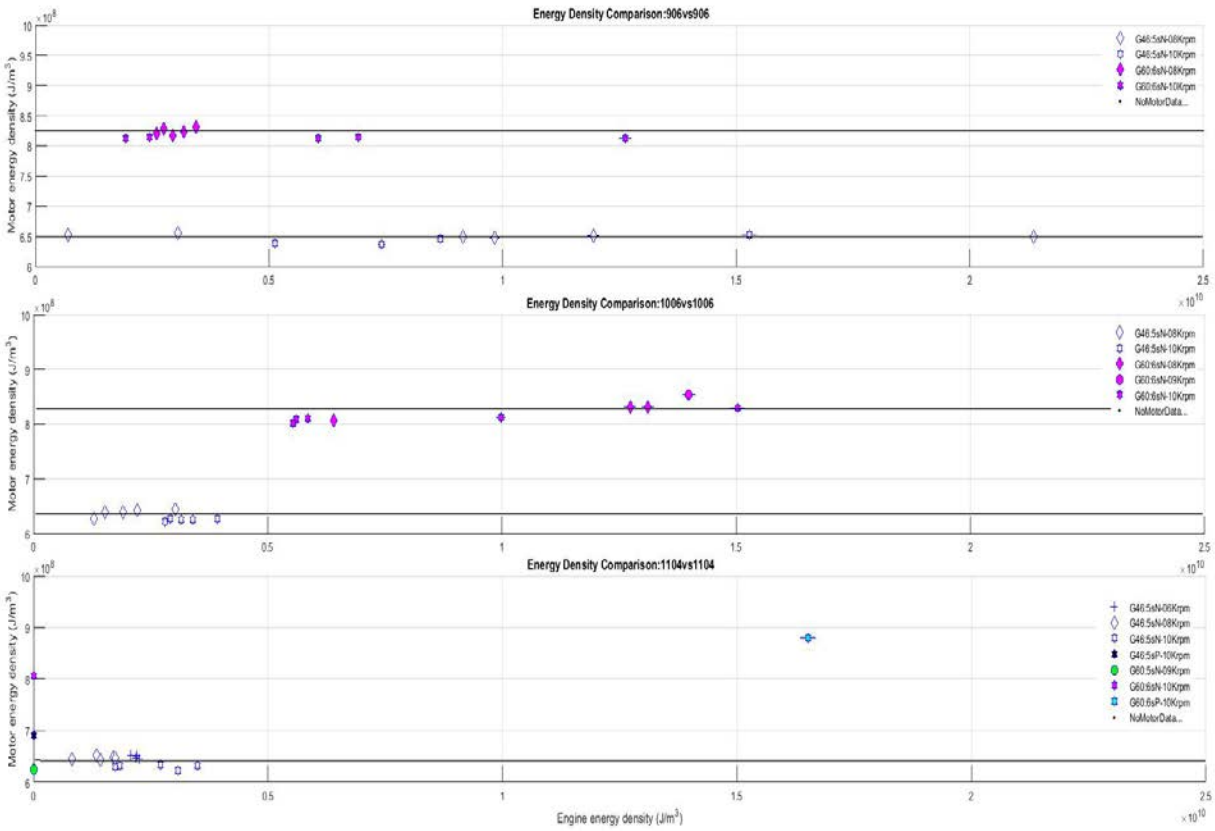

Figure 6.3: Energy Density Comparison for (a) 0906, (b) 1006, (c) 1104

6.1.4: Fuel Flow Rate and BSFC Measurements

Fuel flow rate is the amount of fuel mass used in a time period. Fuel flow rate is crucial in the performance and efficiency of the engine. For this engine, a needle value controls the fuel flow rate. Brake Specific Fuel Consumption (BSFC) is a measure of efficiency and shows improved efficiency as it approaches one. BSFC is a function of fuel flow rate and output power. Therefore, if power is held constant, BSFC will approach one as fuel flow rate decreases. The amount of output power produced is dependent on the air to fuel ratio. The operating conditions for all the test are half throttle (HT), except two that are full throttle (FT), and then the needle value is adjusted until the target speed is confirmed. Figure 6.4 shows the relationship

between BSFC and fuel flow rate. As the fuel flow rate decreases, the engine efficiency increases. Efficiency is increased for the same amount of fuel flow rate if the speed is increased by opening the throttle. Output power is a function of speed. Therefore, for the same fuel flow rate you can achieve greater efficiency. Increasing the efficiency will increase the factor of endurance this research is targeting. Choosing the proper propeller depends on how much power is required. Comparing 1006 and 1104, which has the same output power curve, for optimum conditions shows similar fuel flow rate and BSFC for half throttle and full throttle. Propeller 1006 shows for the same speed (13 Krpm), fuel flow rate and BFSC can be improve by increasing the throttle setting.

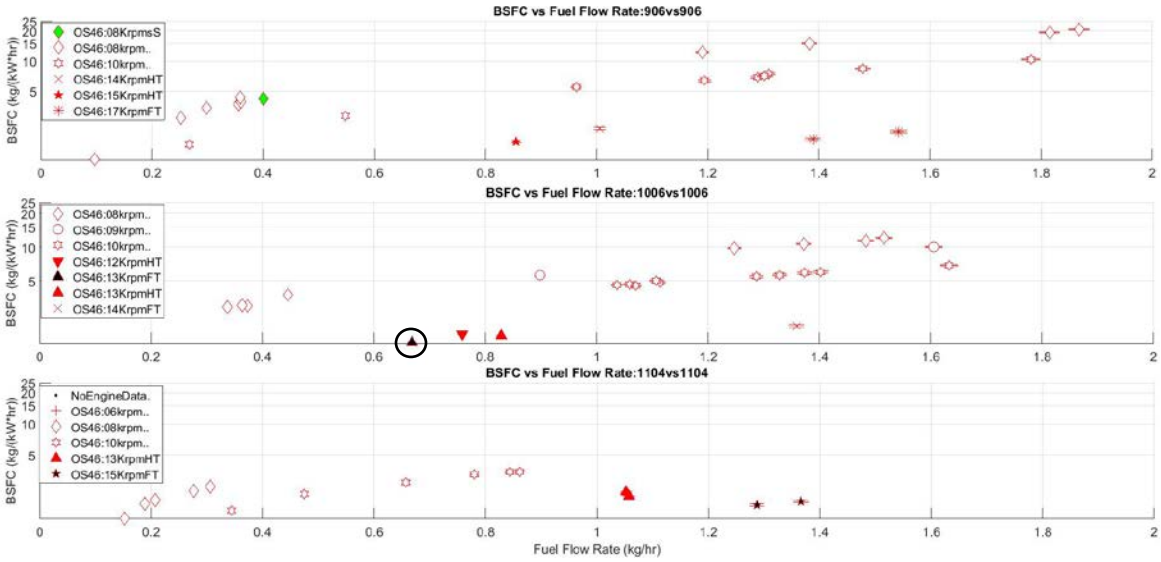

Figure 6.4: BSFC at various fuel flow rates for 0906, 1006, 1104

6.1.5: Efficiency Comparison Measurements

Hydrocarbon powered MAVs usually do not operate to their full potential because its challenging to optimize them based on efficiency parameters. Motor MAVs traditionally are more efficient than these engines because they do not suffer as many

losses: combustion, heat, and friction losses. However, they do suffer from their low specific energy. Thus, for this research, improving the efficiency of the engine is paramount to prove that hydrocarbon power MAVs are even better when optimized. Figure 6.5 is a comparison between the engine and motor efficiencies. As mentioned previous, the engine efficiency when not optimized is in single or low double digits. The spread for the engines measurements is the result of the fuel flow rate being different for each test. Turnigy G46 and G60 motors are used to investigate if the efficiency is improved with increased voltage potential. However, shown in Figure 6.5a and b, the motor size does not change the efficiency. For 8 and 10 Krpm, the efficiencies are approximately 55% and 68% for both motors. The cause of the same efficiencies could be due to the increase in motor size and battery size is linear. Figure 6.5c contains a few interesting cases. First, the 8 and 10 Krpm test are slightly greater at 63% and 89%, The difference is doubled compared to the other propellers. For 6 Krpm, the efficiency is 51%, which is expect from the trend between speed and motor efficiency. Second, a test was performed for each motor with their respective batteries peaked charged. The results show that when the batteries are peaked charged their efficiency is less than nominal charged batteries. This is additional support to not peak charge LiPo batteries even though it increases the endurance by approximately a factor of 4. The process is stressful for the battery, decreases its life cycle, and creates a hazardous environment. Therefore, to increase the efficiency, a

light motor capable of handling a high voltage potential and current would be needed.

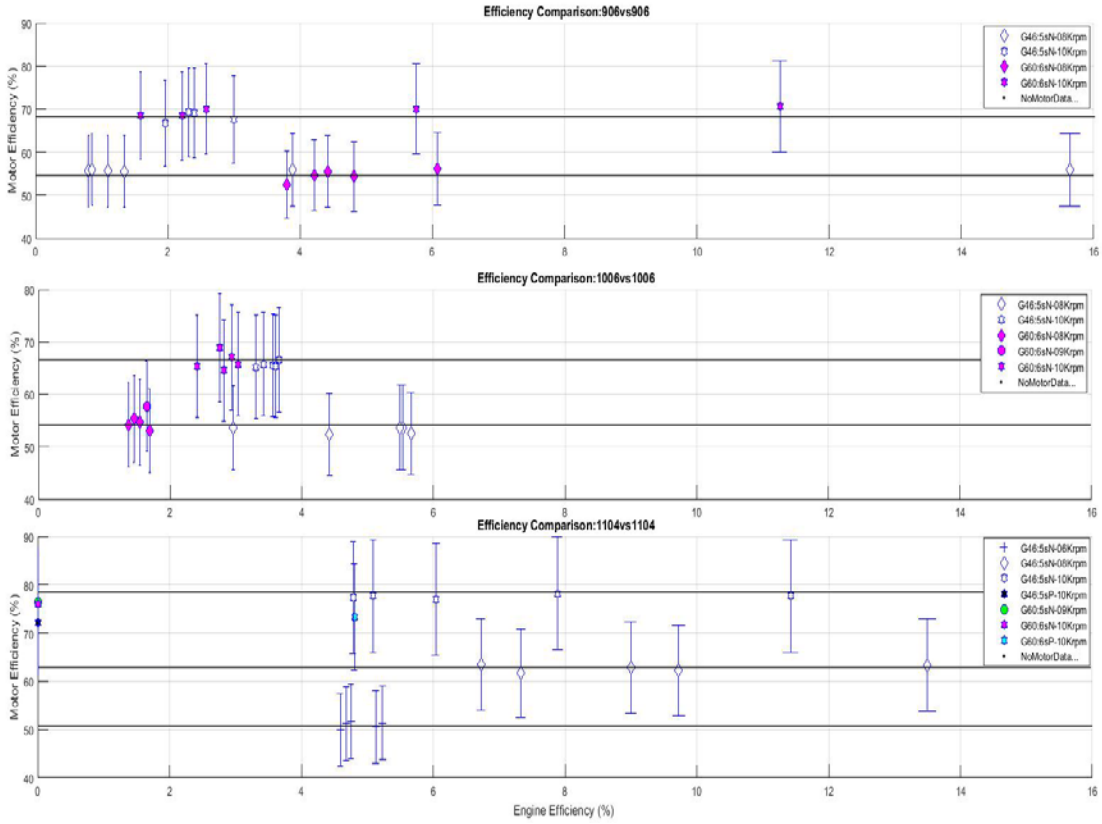

Figure 6.5: Efficiency comparison for (a) 0906, (b) 1006, (c) 1104

6.1.6: Endurance and Efficiency Measurements

As mentioned previous, greater efficiency produces greater endurance. Figure 6.6 compares the endurance ratio and efficiency ratio for the engine and motors. A common trend in Figure 6.6 is the asymptotic curve and decrease in endurance as speed increases. The curve is bounded by the limitation of the motors endurance and the engines efficiency. The decrease in motor endurance is due to higher demand of energy for higher power. The spread in some of the results is due to the slight spread of the engine's fuel flow rate. In figure _a, G46 operating at 8 and 10 Krpm is capable of lasting about half of the engine's duration. At these speed, especially for the 0906,

a high fuel flow rate needs to be administered to achieve the speeds because the propeller is applying a light load. Therefore, the engine efficiency and endurance is not going to be as great as other conditions. For G60, additional fuel is added to the tank because of the additional weight of the motor and battery. The engine would have an endurance factor of 10 and 15 for 8 Krpm and 10 Krpm. The three G60-10 Krpm points between 25 and 45 on the x-axis are the peak charged cases. As mentioned, before they do increase their endurance by a factor of 4. However, at the risk of further deterioration.

Figure 6.6b is similar to Figure 6.6a, but the argument is flipped. G60 is designed to handle higher loads because it has a higher torque rating. Therefore, G60 at 8 and 10 Krpm has a greater endurance and efficiency than the 906 propeller. For the G46, the endurance and efficiency is less than the 906 because it is designed for low loads. However, both motors have greater efficiency than the engine by factors of 10x.

Figure 6.6c, follows the trend of Figure6.6 b, however, 6 Krpm has greater endurance than 8 Krpm. The increase in endurance is due to less demand for energy at this speed. Thus, even though G46 is not designed to swing a large propeller, it is capable of swinging it at low speeds for an extended duration. It should be noted that G46-5sP, G60-9Krpm, and G60-6sN were omitted from this plot because they were ran separate from the engine. Therefore, they show as a value of 0 for this plot. However, G606sP (peak) is shown in cyan and shows the increased endurance compared to nominal charged.

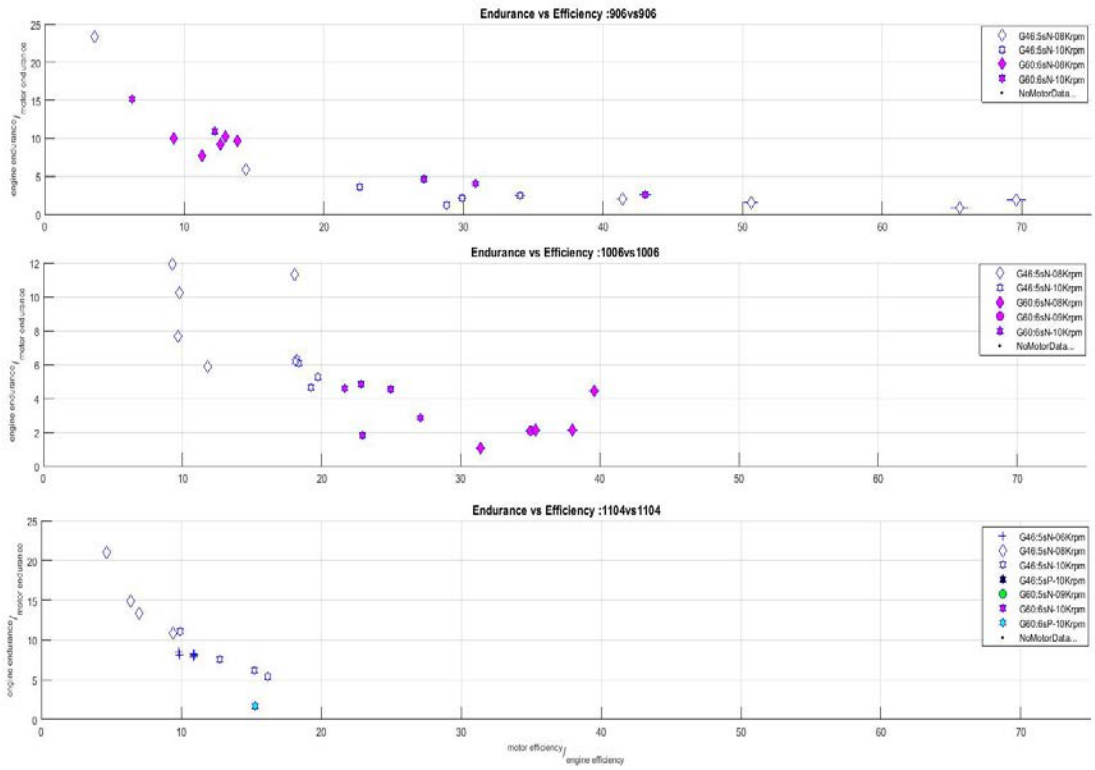

Figure 6.6: Endurance vs Efficiency for (a) 0906, (b) 1006, (c) 1104

6.1.7: Endurance Measurements

Figure 6.7 shows the endurance for the motor and engine for the various propeller, battery, and speed conditions. In the plot, the black dotted line represents if the motor and engine have the same endurance. It is expected that the endurance of the engine will be greater than the motor for all the cases because of the specific energy of the fuel. However, we can see that even for peak charged batteries the engine can operated about twice as long as the motor. For nominally charged, we can see this factor grow.

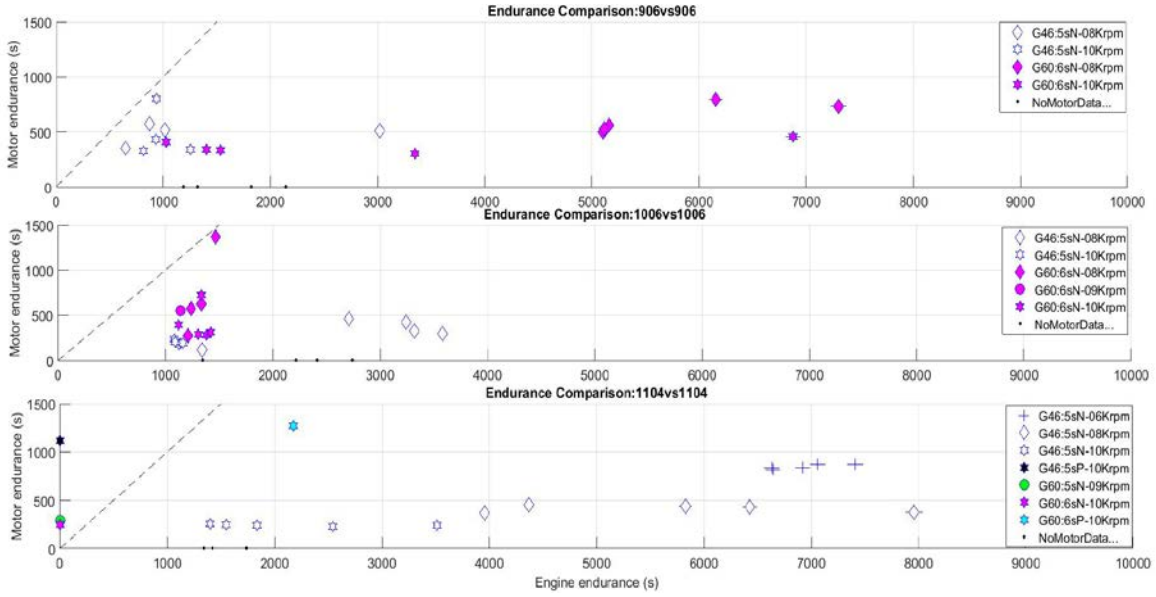

Figure 6.6: Endurance comparison for (a) 0906, (b) 1006, (c) 1104

6.1.8: Effect of Fuel Consumption on Endurance

It must be noted that the endurance calculated in this research is for static conditions because the systems were station on the thrust stand. The following is shows how the endurance ratio for the engine and motor were calculated in the experiments:

$$E_{bat} = P * t_{bat} * \left(\frac{1}{\eta_{o_{motor}}}\right) = E^* * M_{Bat}$$

$$E_{fuel} = P * t_{fuel} * \left(\frac{1}{\eta_{o_{engine}}}\right) = Q_R * M_{fuel}$$

$$\left(\frac{t_{engine}}{t_{bat}}\right)_{exp} = \left(\frac{\eta_{o_{engine}}}{\eta_{o_{motor}}}\right) * \left(\frac{Q_R}{E^*}\right) * \left(\frac{M}{M_{fuel}}\right)$$

where E is the energy, P is the power, t is the endurance, η_o is the overall efficiency, E^* is the specific energy of the battery. Q_R is the lower heating valve (LVH) of the fuel, M_B is the mass of the battery, M_{fuel} is the fuel mass.

To investigate how the endurance will be for when the system is on an aircraft the breguet range equation[27] is used:

$$R_{engine} = \eta_o * \left(\frac{Q_R}{g}\right) * \left(\frac{L}{D}\right) * \ln\left(\frac{M_i}{M_f}\right)$$

where g is gravity, $\frac{L}{D}$ is the lift over drag, M_i is the initial weight, M_f is the final weight. For the engine, the weight of the aircraft is getting lighter throughout the flight because fuel is burned for combustion. However, for the motor, the weight of the system does not change. Therefore, the breguet range equation needs to be modified slightly for batteries[28]:

$$R_{battery} = \eta_o * \left(\frac{E^*}{g}\right) * \left(\frac{L}{D}\right) * \frac{\mathrm{M_{battery}}}{M_f}$$

Endurance is distance over velocity. However, the ratio of the engine and battery endurance is of interest $\frac{t_{engine}}{t_{motor}}$ for when the systems are on an vehicle .

$$\left(\frac{t_{engine}}{t_{motor}}\right)_{Veh} = \left(\frac{\eta_{o\,engine}}{\eta_{o\,motor}}\right) * \left(\frac{Q_R}{E^*}\right) * \frac{\ln\left(\frac{M_{engine}}{M_{f_{engine}}}\right)}{\frac{M_{battery}}{M_{f_{motor}}}}$$

The equation above is the endurance ratio between the engine and the motor for a vehicle. By dividing the vehicle endurance ratio and the experimental endurance ratio a correction coefficient can be found.

$$Correction\ Coeff\ (C) = \frac{\left(\frac{t_{engine}}{t_{motor}}\right)_{Veh}}{\left(\frac{t_{engine}}{t_{bat}}\right)_{exp}}$$

This correction coefficient (C) is applied to find the approximant endurance of the systems when attached to an aircraft (not static).

Figure 6.7 shows this relationship between the correction factor and mass fraction.

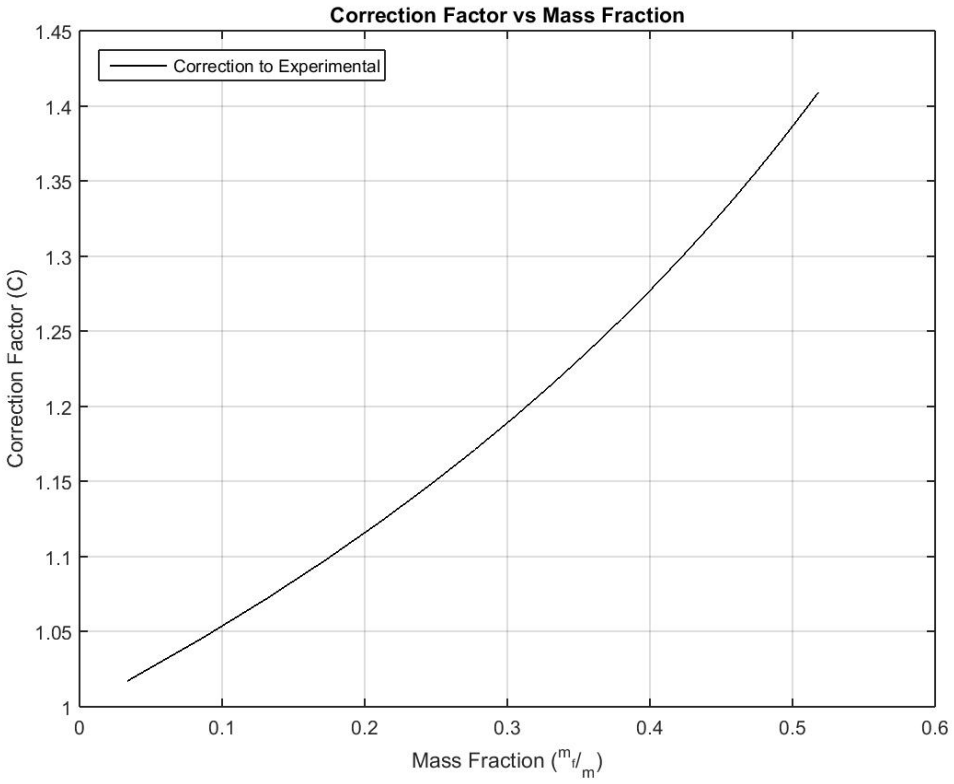

Figure 6.7: Correction Factor for experimental endurance

The mass fraction is the engine mass fraction. The engine mass fraction is correlated to the mass of the battery because both systems must have equal mass. As the weight of the battery is increased the engine mass fraction increases. The solid line in Figure 6.7 represents the correction factor needed to correct the experimental endurance for vehicle endurance. As fuel is added to the system, the correction factor grows exponentially. Therefore, the vehicle endurance grows exponentially. This shows that if the same conditions were repeated with a vehicle the endurance would be greater than the experimental endurance. This highlights the benefit of using fuel instead of

batteries because batteries do not decrease in mass, which causes a decrease in endurance. In this case of the 5S and 6S batteries, the correction coefficient are 1.1968 and 1.281.

Chapter 7: Conclusion

Various test was produced for different cases between the engine and motors. Speed, temperatures, tank pressures, and thrust were measured for all test. Fuel flow rate, power, energy density, power density, and efficiencies were calculated for all test. A operating performance map was generated between the OS 46 AX II and Master Airscrew propellers to determine the best propellers to use for this engine. After analyzes, it is determined that the KN1006 is the best propeller for this engine. The KN0906 allows the engine to operate in the majority of the speed spectrum. However, it was difficult achieve the optimized engine point of speed=14 Krpm, power= 471 W, and efficiency= 12.41. The closest points achieved are shown below:

```
>> [avg_eRPM' e_proppower' e_eff' tot_dur']
ans =
       8152.4        94.26       3.8881       3018.1
        13983       474.34        7.782       1363.3
        14615       541.78       10.452       1603.1
```

(0906 5s)

```
>> [avg_eRPM' e_proppower' e_eff' tot_dur']
ans =
       8152.4        94.26       3.8881       3018.1
        13983       474.34        7.782       1823.4
        14615       541.78       10.452       2144.2
```

(0906 6s)

```
>> [avg_eRPM' e_proppower' e_eff' tot_dur']
ans =
       7979.8       119.32       4.4232       2712.3
       12661       477.09       11.779       2051.6
       14321       690.15       8.3756       1008.5
```
(1006 5s)

```
>> [avg_eRPM' e_proppower' e_eff' tot_dur']
ans =
       7979.8       119.32       4.4232       2712.3
       12661       477.09       11.779         2744
       14321       690.15       8.3756       1348.8
```
(1006 6s)

Considering the KN1104 outputs the same power and thrust, the KN1006 allows the engine to operate in prime regimes. From the operating performance map, the operating point is: speed=12 Krpm, power=393.1 W, and efficiency=12.9. The KN1006 is the closest with speed=13 Krpm, power=405 W, and efficiency =12. This condition is achieved when the engine is operating at full throttle, which enables for four times as much endurance compared to non-optimized conditions. With this data, commercial consumers are will be able to optimize their person engine and receive the best performance. In addition, this will also promote personal financial interest as one gallon of fuel is around $27. The optimum condition has the lowest fuel flow rate. Therefore, it not only increases endurance, but decreases the need to purchase an excessive amount of fuel. In military aspect, this engine can be applied rather than electric motors to carry surveillance and tactical missions. The outcome will have greater endurance and the possibility of carrying heavier loads for deliveries or equipment. This research proves that even for an un optimized engine hydrocarbon fuels are still necessary to provide greater endurance and power. Then, when the engine is optimized by propeller matching and fuel to air configurations, the engine is

capable of performing better by a factor of 4. Lastly, a correction coefficient plot was generated, which emphasizes that if the systems are applied to vehicles the engine's endurance would continue to increase because it the fuel weight decreases.

Chapter 8: Future Work

The test performed were all for static conditions. It would be interesting to see how the engine and motors would perform in flight testing. A fuselage of equal mass could be constructed to house all the instrumentation and inserted in a wind tunnel. Running flight simulations would properly gauge how the systems would operate in realistic conditions. Also, there is no data for the motors because the company did not produce them. Characterizing the motors using a dynamometer would provide useful data to construct a motor performance map. Similar to the engine performance map, an optimum operating map can be made with various propellers. Another set of test can be performed finding the best propeller for the motor. Then, the engine and motors can compete while running at optimum settings. The OS 46 AX II currently operates with glow fuel as its hydrocarbon fuel. Glow fuel is about seven times as expensive than gasoline and has half the amount of specific energy. Purchasing a converter for the OS 46 to operate using gasoline is an area that should be explored especially for military applications. It could be inferred gasoline would increase the endurance and power of a non-optimized engine by a factor of two and a optimized engine by eight. Lastly, utilizing the data from this thesis and future work to apply a variable pitch propeller to optimized the engine for specified parameters and external conditions. A

variable pitch propeller would allow the engine to sweep through various operating ranges, thus making the engine's performance robust.

Appendix

If needed.

Glossary

If needed.

Cited Work

1. Joe Martin Foundation. Model Airplane Engine Designers and Builders. Available at: http://www.craftsmanshipmuseum.com/enginemen.htm. (Accessed: 27th November 2017)

2. Academy of Model Aeronautics. Academy of Model Aeronautics - AMA History Program - Completed Biography List. Available at: http://www.modelaircraft.org/museum/biolist.aspx. (Accessed: 27th November 2017)

3. NOVA. NOVA | Spies That Fly | Time Line of UAVs | PBS. Available at: http://www.pbs.org/wgbh/nova/spiesfly/uavs.html. (Accessed: 27th November 2017)

4. Menon, S. K. The scaling of performance and losses in miniature internal combustion engines. *ProQuest Diss. Theses* **3443486,** 459 (2010).

5. Cadou, C., Moulton, N., Aluko, M., Sookdeo, T. & Leach, T. Performance Measurement and Scaling in Small Internal Combustion Engines. *41st Aerosp. Sci. Meet. Exhib.* 1–11 (2003). doi:10.2514/6.2003-671

6. Menon, S. & Cadou, C. P. Scaling of Miniature Piston-Engine Performance, Part 1: Overall Engine Performance. *J. Propuls. Power* **29,** 774–787 (2013).

7. Menon, S. . & Cadou, C. P. . Scaling of miniature piston engine performance Part 2: Energy losses. *J. Propuls. Power* **29,** 788–799 (2013).

8. Deters, R. W., Ananda, G. K. & Selig, M. S. Reynolds Number Effects on the Performance of Small-Scale Propellers. (2014).

9. Brandt, J. B. & Selig, M. S. Propeller Performance Data at Low Reynolds Numbers. (2011).

10. John B. Brandt, Robert W. Deters, Gavin K. Ananda, and M. S. S. UIUC Propeller Data Site. Available at: http://m-selig.ae.illinois.edu/props/propDB.html.

11. Menon, S. K. The scaling of performance and losses in miniature internal combustion engines. *ProQuest Dissertations and Theses* **3443486,** (2010).

12. Collair, K. & Floweday, G. Understanding HCCI Characteristics in Mini HCCI Engines. *SAE Tech. Pap.* 4 (2008). doi:10.4271/2008-01-1662

13. Hebert, I. Otto Cycle. 2–4 (2017). Available at: http://ffden-2.phys.uaf.edu/212_fall2009.web/Isaac_Hebert/Otto_Cycle.html.

14. Brushing Up on Brushless. Available at: http://www.toolsofthetrade.net/power-tools/cordless-tools/brushing-up-on-brushless_o. (Accessed: 3rd October 2017)

15. Brushless motors - how they work and what the numbers mean - Guides - DroneTrest. Available at: http://www.dronetrest.com/t/brushless-motors-how-they-work-and-what-the-numbers-mean/564. (Accessed: 3rd October 2017)

16. Rahn, C. *Battery System Engineering*. *Traffic Safety* **22,** (2013).

17. National Instruments. NI 9205 Datasheet. (2015). Available at: http://www.ni.com/pdf/manuals/374188a_02.pdf. (Accessed: 5th October 2017)

18. Instruments, N. NI 9213 Datasheet. Available at: http://www.ni.com/pdf/manuals/374916a_02.pdf. (Accessed: 5th October 2017)

19. Instruments, N. NI 9401 Datasheet. Available at: http://www.ni.com/pdf/manuals/374068a_02.pdf. (Accessed: 5th October 2017)

20. Additional, F. & See, I. PX277 Manual. 275–278 Available at: https://www.omega.com/manuals/manualpdf/M2759.pdf#search=px 277.

21. OMEGA. LCM703. (2016). Available at: https://www.omega.com/pptst/LCM703.html.

22. Transducer Technique. LSP Series low capacity single point bending beam Load Cells. Available at: https://www.transducertechniques.com/lsp-load-cell.aspx.

23. Engine, O. 46AX II ABL. 7974 (2000). Available at: http://www.osengines.com/engines-airplane/osmg0548/index.html.

24. Mcclimon, M. Test Uncertainty. *Writing* **2005,** 1–3 (2014).

25. UMN.edu. Understanding DC Motors. Available at:

http://www.me.umn.edu/courses/me2011/arduino/technotes/dcmotors/motor-tutorial/. (Accessed: 5th December 2017)

26. Natural Resources Canada. Principles of Operation - AC VFD Drives. Available at: http://www.nrcan.gc.ca/energy/products/reference/15433. (Accessed: 5th December 2017)

27. MIT. 13.3 Aircraft Range: the Breguet Range Equation. Available at: http://web.mit.edu/16.unified/www/FALL/thermodynamics/notes/node98.html. (Accessed: 1st December 2017)

28. Hepperle, M. Electric Flight – Potential and Limitations Abbreviations and Symbols.